

NASA TECHNICAL MEMORANDUM

NASA TM-82404

WELD GEOMETRY STRENGTH EFFECT IN 2219-T87 ALUMINUM

By A. C. Nunes, Jr., H. L. Novak,
and M. C. McIlwain
Materials and Processes Laboratory

March 1981

NASA



*George C. Marshall Space Flight Center
Marshall Space Flight Center, Alabama*

(NASA-TM-82404) WELD GEOMETRY STRENGTH
EFFECT IN 2219-T87 ALUMINUM (NASA) 47 p
HC A03/MF A01 CSCL 11F

N81-21172

Unclas
G3/26 41971

TECHNICAL REPORT STANDARD TITLE PAGE

1. REPORT NO. NASA TM-82404		2. GOVERNMENT ACCESSION NO.		3. RECIPIENT'S CATALOG NO.	
4. TITLE AND SUBTITLE Weld Geometry Strength Effect in 2219-T87 Aluminum				5. REPORT DATE March 1981	
				6. PERFORMING ORGANIZATION CODE	
7. AUTHOR(S) A. C. Nunes, Jr., H. L. Novak, and M. C. McIlwain				8. PERFORMING ORGANIZATION REPORT #	
9. PERFORMING ORGANIZATION NAME AND ADDRESS George C. Marshall Space Flight Center Marshall Space Flight Center, Alabama 35812				10. WORK UNIT NO.	
				11. CONTRACT OR GRANT NO.	
				13. TYPE OF REPORT & PERIOD COVERED Technical Memorandum	
12. SPONSORING AGENCY NAME AND ADDRESS National Aeronautics and Space Administration Washington, D. C. 20546				14. SPONSORING AGENCY CODE	
15. SUPPLEMENTARY NOTES Prepared by Materials and Processes Laboratory					
16. ABSTRACT <p>A theory of the effect of geometry on the mechanical properties of a butt weld joint is worked out based upon the soft interlayer weld model. Tensile tests of 45 TIG butt welds and 6 EB beads-on-plate in 1/4-in. 2219-T87 aluminum plate made under a wide range of heat sink and power input conditions are analyzed using this theory. The analysis indicates that purely geometrical effects dominate in determining variations in weld joint strength with heat sink and power input. Variations in weld dimensions with cooling rate are significant as well as with power input. Weld size is suggested as a better indicator of the condition of a weld joint than energy input.</p>					
17. KEY WORDS			18. DISTRIBUTION STATEMENT Unclassified--Unlimited		
19. SECURITY CLASSIF. (of this report) Unclassified		20. SECURITY CLASSIF. (of this page) Unclassified		21. NO. OF PAGES 45	22. PRICE NTIS

ACKNOWLEDGMENTS

The authors wish to express their appreciation for special assistance provided by NASA co-workers. C. A. Brosemer did much of the weld preparation work. M. W. Brennecke contributed expertise in the area of aluminum metallurgy. P. M. Munafa's suggestions for improving Appendix A are incorporated. The authors are also indebted to R. A. Chihoski of Martin-Marietta Aerospace for discussions leading to the initiation of this study.

TABLE OF CONTENTS

	Page
INTRODUCTION	1
TEST PROCEDURES.....	2
TEST RESULTS.....	3
DISCUSSION.....	10
CONCLUSIONS.....	19
REFERENCES	20
APPENDIX A.....	22
APPENDIX B.....	37

LIST OF ILLUSTRATIONS

Figure	Title	Page
1.	Bar graphs of weld tensile test results.....	4
2.	Typical hardness distributions around TIG and EB welds.....	6
3a.	Electron beam weld fracture surface (x500).....	7
3b.	Electron beam weld fracture (x5).....	7
4a.	TIG weld fracture-heat sinked (x5).....	8
4b.	TIG weld fracture-no heat sink (x5).....	8
5.	TIG weld fracture-heat sinked (x5).....	9
6.	TIG weld fracture-no heat sink (x5).....	9
7.	Effect of root pass power (current) and heat sink capacity on weld size.....	11
8.	Effect of root pass energy on root width and root drop.....	12
9.	Comparison of data from Reference 14 with calculated dependence of yield stress and ultimate tensile strength on weld size parameter.....	14
10.	Effective versus measured weld size parameters.....	14
11.	Yield stress and ultimate tensile strength data versus effective weld size parameter.....	15
12.	Weld size parameter corrections for yield stress and ultimate tensile strength.....	17
13.	Interpretation of weld test data using soft interlayer weld model.....	18
A-1.	Soft interlayer weld model.....	23
A-2.	Yield stress of soft interlayer joint.....	24
A-3.	Equivalent width of weld.....	25

LIST OF ILLUSTRATIONS

Figure	Title	Page
A-4.	Development of plastic flow field in soft interlayer under tension. Slip-lines, along which slip takes place, are shown	26
A-5.	Geometry and boundary conditions assumed for Prandtl analysis of fully developed plastic flow field.....	27
A-6.	Mohr's circle for stress transformation of yielding element.....	28
A-7.	Comparison of tensile stress amplification factor for soft interlayer as a function of weld width to plate thickness ratio calculated by Prandtl and slip-line field analyses.....	34
A-8.	Strength of weld joint obtained from strength of parent and weld metal using a simplified soft interlayer weld model	35

TECHNICAL MEMORANDUM

WELD GEOMETRY STRENGTH EFFECT IN 2219-T87 ALUMINUM

INTRODUCTION

The strength of a weld joint is determined in part by the mechanical properties of the joint materials, i.e. parent metal, fusion zone metal, and heat-affected-zone metal, and in part by the geometry of the joint. In order to understand the results of weld experiments and to use these results to design better welds, it is desirable to distinguish between purely geometrical strength effects and effects due to microstructural transformations going beyond mere widening or narrowing of the weld zone.

For metals like 2219-T87 aluminum, the weld zone comprises a relatively soft region bounded by appreciably harder parent metal. Observations reported in this report suggest that the geometrical effect on the strength of such a weld can be understood in terms of a soft interlayer model [1,2,3].

In the soft interlayer weld model the weld is treated as a uniform layer of soft material between two hard, flat plate ends. The weld is taken to be very long. The geometry of the soft interlayer is characterized by a single parameter: the ratio of weld or layer width to plate or layer thickness.

For weld widths greater than the plate thickness little constraint is exerted on the soft weld metal. The weld metal yields, reaches its ultimate tensile strength, and ruptures about as it would if it constituted the entire plate. The yield stress and ultimate tensile strength of the weld joint are the same as that of the soft metal in this circumstance.

Constraints on the flow of the soft weld metal raise the yield stress and ultimate tensile strength of the weld joint above that of the weld metal when the weld width is less than the plate thickness [4]. By making the weld sufficiently narrow, joint strength can be raised to that of the parent metal [2,3]. While constraints on soft weld metal flow raise the weld joint strength, a triaxial tensile stress is created in the center of the weld zone. If the tensile stress exceeds the fracture stress of the weld metal, then the weld ruptures [5]. The fracture stress depends upon the flaw size and the fracture toughness of the soft weld metal [6].

The hardness [7] and fracture toughness [8,9,10] of the weld zone in 2219-T87 aluminum are both functions of thermal history and the resultant distribution of particle inclusions, which act as barriers to dislocation motion as well as nucleation and arrest sites for cracks. The size of the weld zone is also a function of thermal history.

In the course of specimen preparation for this study it was made abundantly clear that cooling rate of the weld environment as well as energy input determines the thermal history of the weld. This observation is in line with an earlier study [11] in which fixture clamping pressure variations along a 1/4-in. aluminum plate produced visible variations in weld penetration depth.

B. L. Shultz and C. E. Jackson [12] were led by difficulties in characterizing the thermal history of a weld to propose a geometrical (weld bead area) indicator in preference to energy input per unit length of weld. They state: "Since various cooling rates can be obtained for a given welding energy input, the energy input concept cannot adequately predict mechanical properties."

Welders also tend to give priority to weld geometry over weld process parameters. It is common practice to adjust weld heat (current) from workpiece to workpiece and even along the same bead so as to maintain constant weld dimensions.

Pending further work, it appears that the variations in butt weld mechanical properties correlate directly with the ratio of weld width to plate thickness. Furthermore the soft interlayer weld model allows purely geometrical effects to be separated from metallurgical (microstructural) effects other than alteration of soft weld zone width. Results obtained from the present study indicate that it is the purely geometrical effects which dominate in determining the behavior of butt weld joints in 1/4-in. 2219-T87 aluminum plate.

TEST PROCEDURES

A set of three tensile specimens for each of 15 different weld power / heat sink combinations, or a total of 45 weld specimens, were prepared and tensile tested. After elimination of four specimens due to testing procedure errors, 41 specimens remained to yield the reported results.

Specimens for this study were made from 1/4-in. thick 2219-T87 aluminum joined with multipass, square butt, gas-tungsten arc (GTA) welds. Filler wire, when required, was 2319 aluminum. First the plates were joined by a penetration root pass without use of filler wire. A 1/8-in. diameter 2 percent thoriated tungsten electrode at 12.5 V dc straight polarity was used. The weld speed was 9 in./min. Helium gas shielding at 90 ft³/hr was used. Power input was varied by varying current flow over a range of 120 to 315 A.

Second, from one to three filler passes at 14 or 14.5 V and 120 to 155 A with wire feed rates ranging from 6 to 35 in./min were used. Weld speed and helium gas flow remained at 9 in./min and 90 ft³/hr as for the root pass.

Weld conditions were held for 8-in. intervals. This allowed three different welds per pair of panels. Finished welds were inspected visually and radiographed for internal flow detection. All specimens used were free of internal or external flaws within the sensitivity of the tests. Weld surfaces were left as welded with crown heights from 0 to 0.075 in. and root drops from 0 to 0.112 in.

Tensile specimens approximately 1/4-in. thick by 1-in. wide by 10-in. long were cut (saw cuts machined smooth) across the welds in the stabilized weld zones. Metallographic observations were made before and after tensile testing. Microhardness measurements were made across several untested weld cross sections.

For minimum heat sink conditions panels were isolated from the clamping fixture by fiberglass tape. For maximum heat sink conditions a special clamping fixture was made. The maximum heat sink fixture consisted of machined aluminum plates bolted to a sub-plate and sandwiching the test panels.

For comparison purposes, to show the effect of substantial reduction in weld thickness, two electron beam welds (beads on plate) were tested. Three 1/4-in. thick 2219-T87 aluminum plates were clamped together in a sandwich. The plates were subjected to an electron beam just penetrating into the lower plate. The plates were machined apart and the weld surfaces machined flush. The bottom plate was discarded, the middle plate contained a thin weld, and the top plate, with the EB weld nailhead, contained a thicker weld.

Three unwelded parent metal specimens, with the same geometry as the weld specimens in the gage cross section, were also tested.

TEST RESULTS

The elongations, yield stresses, and ultimate tensile strengths obtained for the welds tested are displayed in Figure 1.¹ The values for the TIG welds are summarized in Table 1.

The results are displayed against a weld size parameter, $(W_R + W_T) / 2t$, the mean weld width (weld root width W_R plus weld top width W_T divided by two) divided by the plate thickness.

TIG-welded specimens welded in high heat capacity fixtures are distinguished from those welded in low heat sink capacity fixtures.

1. Figure 1 is constructed by connecting the tops of bar graphs to emphasize trends and eliminating the vertical lines delineating the bars, which in themselves do not add to the information conveyed.

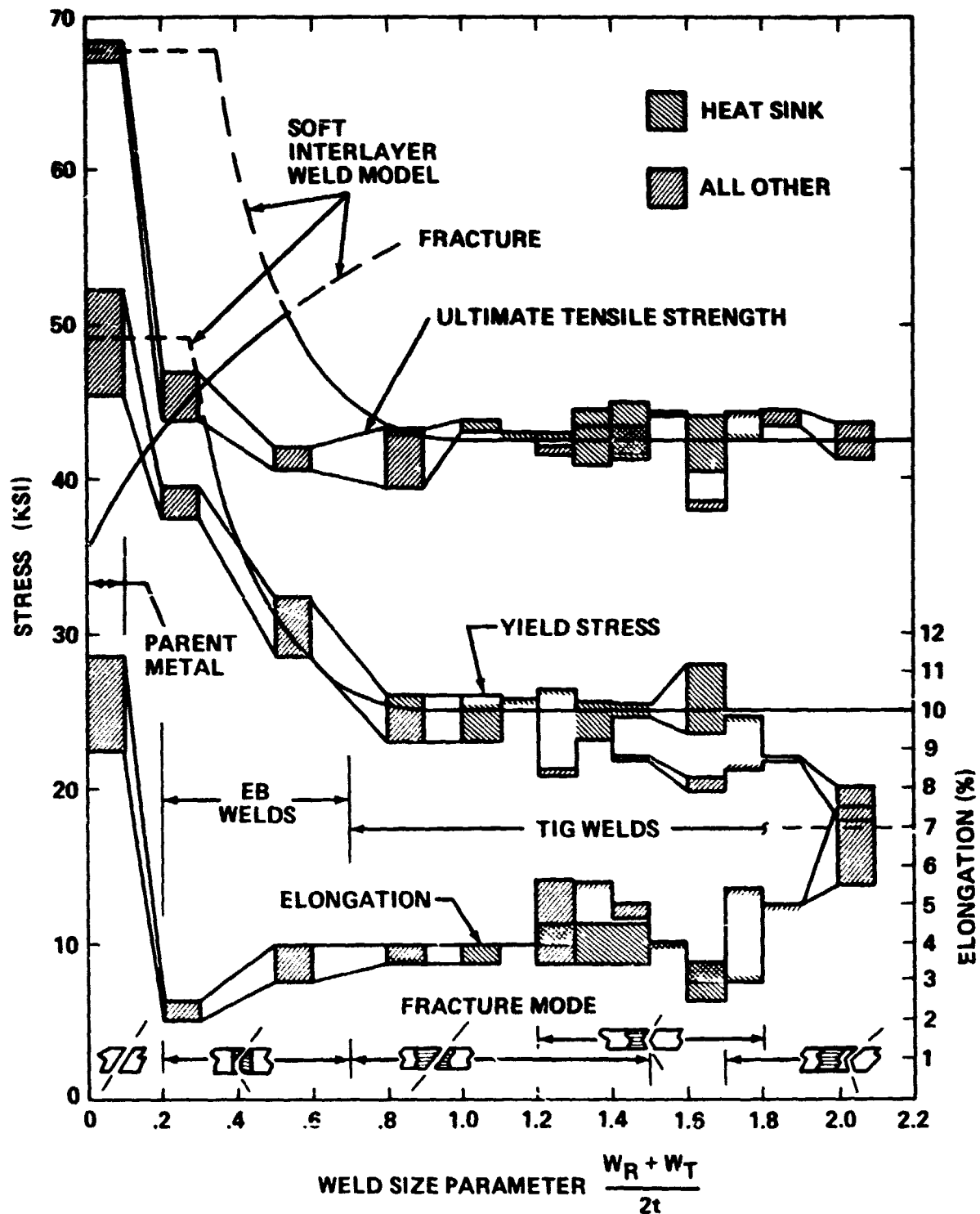


Figure 1. Bar graphs of weld tensile test results.

TABLE 1. TIG WELD STRENGTH PROPERTIES

	Elongation (percent)	Yield Strength (ksi)	Ultimate Tensile Strength (ksi)
Maximum	7.5	27.0	44.6
Mean	4.1	25.2	42.6
Minimum	2.5	17.9	38.3
Standard Deviation	1.0	2.8	1.7

Hardness distributions in a TIG and in an EB weld are displayed in Figure 2. The approximate flow stress corresponding to the hardness is indicated at right. Note that the hardness distributions are similar, the only outstanding difference being in relative widths. The TIG weld is substantially wider than the EB weld. The heat-affected-zone of the EB weld is larger in proportion to its fusion zone than the heat-affected-zone of the TIG weld. This implies that the weld size parameters of the narrower fusion zones should be increased somewhat (roughly around 30 percent for the narrowest EB weld) for better correspondence with the theory of weld geometry effect on strength developed in Appendix A.

The maximum approximate flow stress outside the weld corresponds roughly (75 ksi from hardness measurements versus 68 ksi ultimate tensile strength, a difference of 9 percent) to the ultimate tensile strength of the parent metal. The approximate mean flow stress of the fusion zone for either weld is about 38 ksi, 11 percent lower than the mean ultimate tensile strength of the TIG welds and presumably of the weld metal itself.

Figures 3 through 6 display the types of fractures observed. Shear fractures on 45 degree slip planes are observed in the unwelded parent metal and in the weld fusion zone for the TIG welds of widths up to 1.5 times the weld thickness. Wider TIG welds show fusion line fractures, i.e., fractures along the boundary between the fusion zone and the heat-affected-zone, which transform to heat-affected-zone fractures at weld widths between 1.7 to 1.8 times the plate thickness. Fusion line fractures begin to show up at weld widths as low as 1.2 times the plate thickness, in mixtures with the 45 degree fusion zone fractures which are still occurring at this width.

The EB weld fractures display both straight across and angled fracture portions. The weld fracture surface shows dimples indicating ductile fracture.

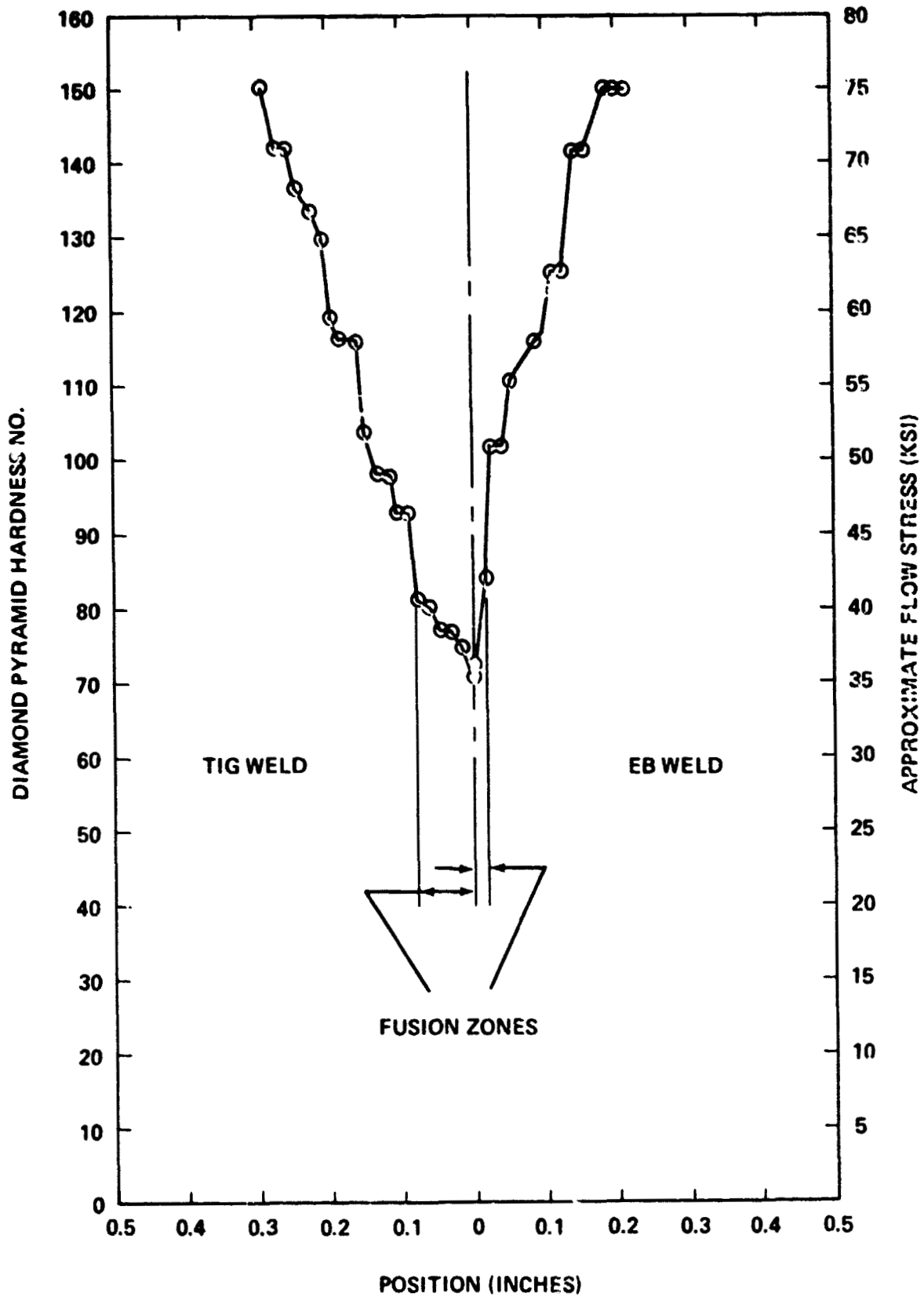


Figure 2. Typical hardness distributions around TIG and EB welds.

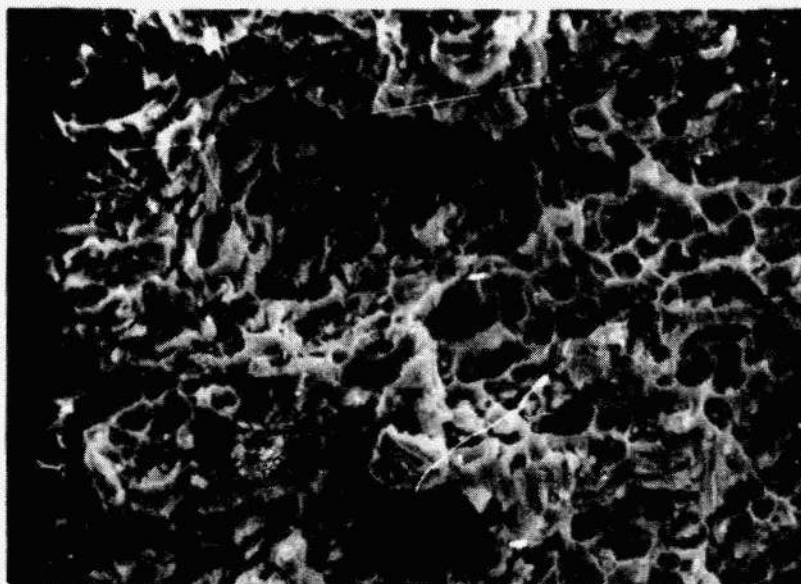


Figure 3a. Electron beam weld fracture surface (x500).

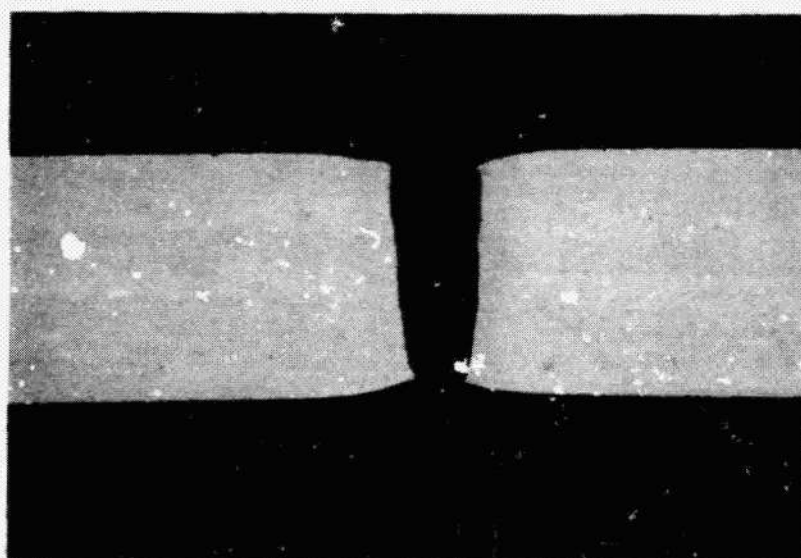


Figure 3b. Electron beam weld fracture (x5).

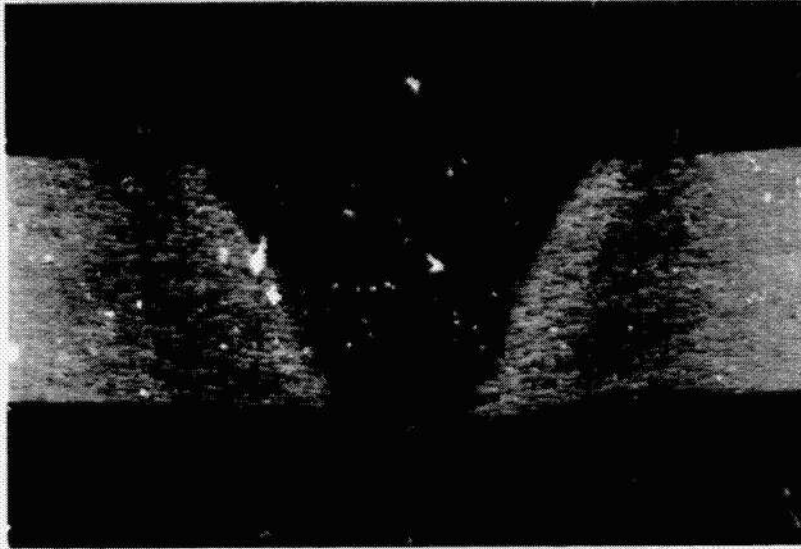


Figure 4a. TIG weld fracture-heat sinked (x5).

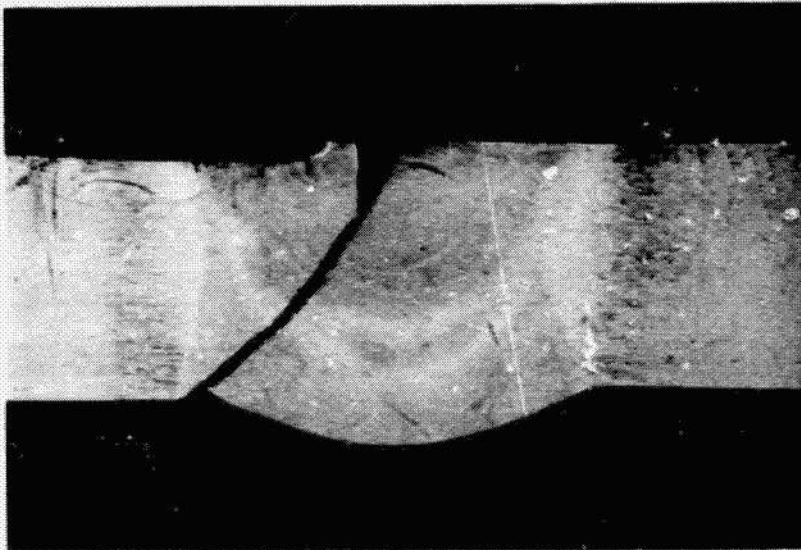


Figure 4b. TIG weld fracture-no heat sink (x5).



Figure 5. TIG weld fracture-heat sinked (x5).

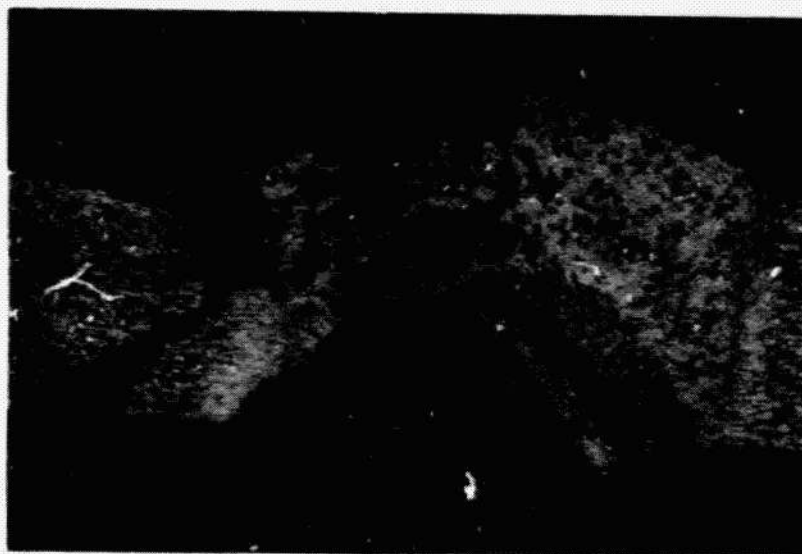


Figure 6. TIG weld fracture-no heat sink (x5).

ORIGINAL PAGE IS
OF POOR QUALITY

Figures 7 and 8 show that weld cooling rate, as controlled by heat sink capability of the weld fixture, affects weld geometry (and, this implies, other weld characteristics also) to an extent that cannot be ignored if weld properties are to be characterized. It should be noted that contact resistances between fixtures and workpieces are both hard to estimate and subject to variation, so that although the measured effects have been exaggerated by the experimental procedure, real, significant effects should be expected in practice [1].

Figure 7 shows the effect of root pass current (the major energy input to the weld) on weld size. For a weld as wide as the plate thickness raising the heat sink capacity from minimum to maximum requires a 50 A (38 percent) rise in current to maintain width.

Figure 8 shows the effect of root pass energy per unit length of weld on weld root contours. Lowering the heat sink capacity from maximum to minimum raises a root width of 0.02 in. to 0.20 in. (900 percent) without changing energy input, which is often treated as a weld constant used to set preliminary weld process parameters!

DISCUSSION

The yield stress dependence of the weld joint on weld size parameter agrees well with the soft interlayer weld model worked out in Appendix A, particularly if the weld size parameter of the narrowest EB weld is advanced by around 30 percent to account for proportionately greater heat-affected-zone width. No metallurgical (microstructural) alteration of the weld metal need be postulated except for very wide welds 1.5 times the plate thickness and wider. These welds appear to show the effect of a heat-affected-zone becoming softer than the fusion zone. The yield stress starts to drop off, the elongation goes up, and the fracture relocates to the heat-affected-zone.

The ultimate tensile strength agrees qualitatively with the soft interlayer weld model of Appendix A, but does not rise as does the yield stress. If the failure to rise is due to the onset of fracture, equation (A35) of Appendix A computes fracture stresses of 56 and 70 ksi for the wider and narrower EB welds respectively. These stresses exceed the ultimate tensile strength of the unconstrained weld metal and are not impossible.

The fracture toughness K_{Ic} of the weld metal may be estimated very tentatively from the appearance of the ductile fracture surface [13]:

$$K_{Ic} \approx \sqrt{\frac{\sigma_u h_o E}{2}} \quad (1)$$

W_R = WELD ROOT WIDTH
 W_T = WELD TOP WIDTH
 t = PLATE THICKNESS

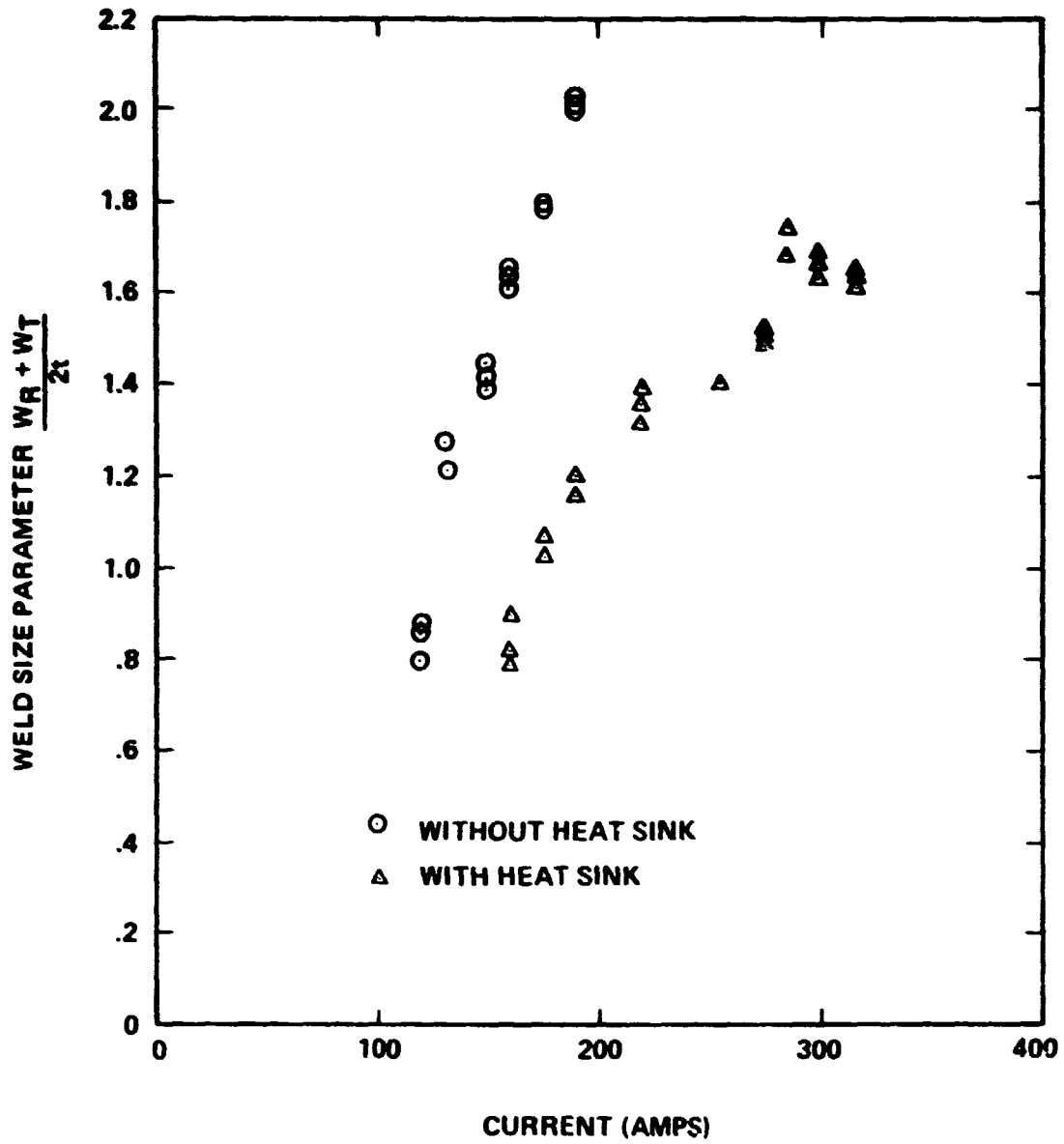


Figure 7. Effect of root pass power (current) and heat sink capacity on weld size.

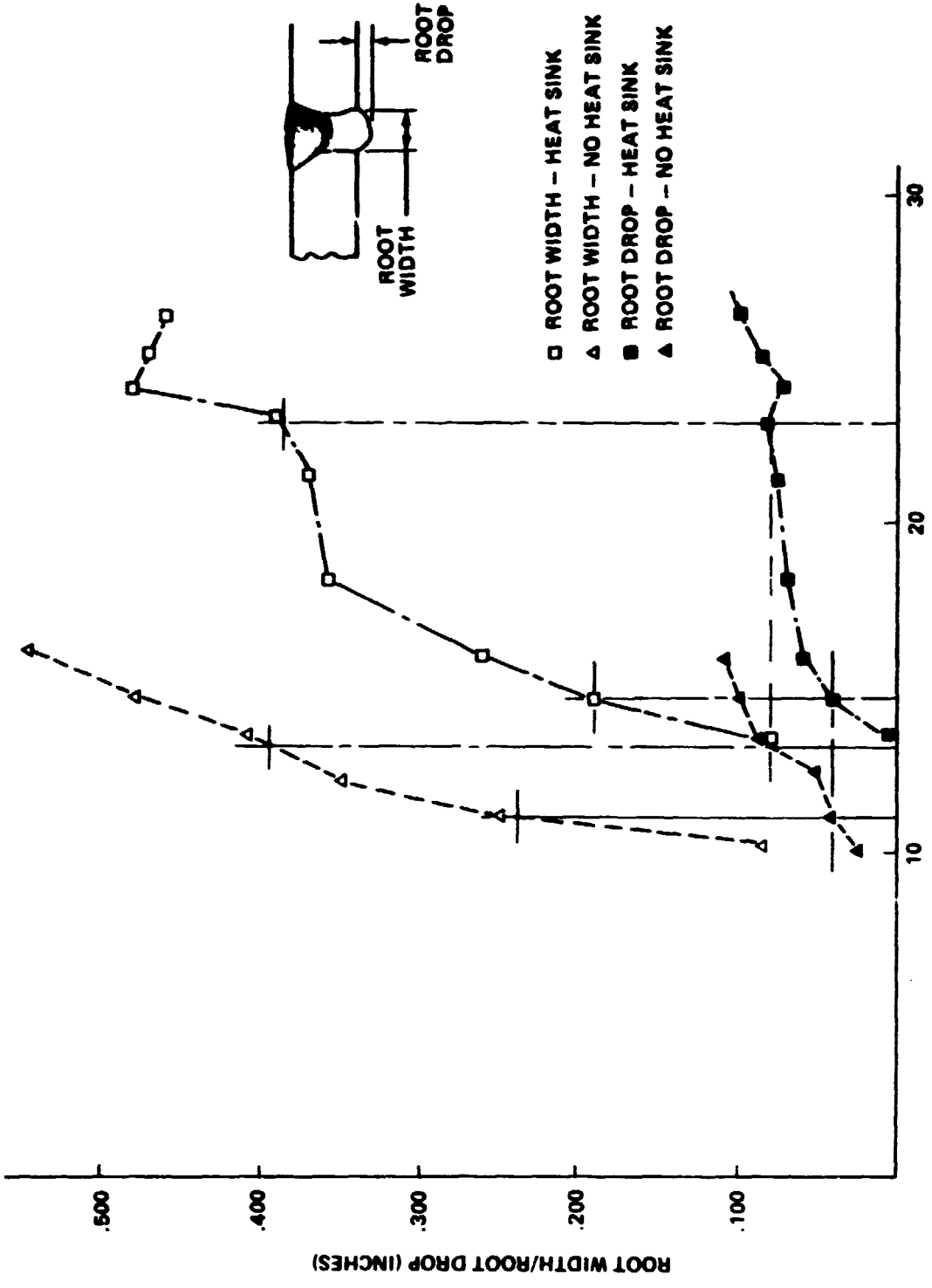


Figure 8. Effect of root pass energy on root width and root drop.

where E is the elastic modulus of the metal (10.7×10^6 psi), and h_o is the height of the edges of the larger dimple patterns on the fracture surface. h_o is estimated to be about the same as the diameter of the corresponding dimple pattern. Estimating h_o at about 0.002 in. from Figure 3a, fracture toughnesses of 21 and 22 $\text{ksi}\sqrt{\text{in}}$ are computed for the wide and narrow EB welds respectively. These may be compared with 42.6 $\text{ksi}\sqrt{\text{in}}$ listed for 2219-T81 aluminum in the Aerospace Structural Materials Handbook.

For a circular crack of radius a in a large body in tension perpendicular to the crack the stress intensity factor is given by:

$$K = 2 \sigma \sqrt{\frac{a}{\pi}} \quad (2)$$

Using equation (2) to compute the critical flaw radius required to produce the very tentatively estimated critical stress intensities or fracture toughnesses, critical flaw radii of 0.11 and 0.08 in. are calculated. These flaws are large and would presumably have been detected during inspection. Thermal stresses during welding or contamination from the sandwich interface may have generated defects in the EB weld specimens somewhat different from what would be encountered in a more conventional EB weld joint.

Some additional EB weld data on heavy gage aluminum alloys obtained from M. W. Brennecke [14] are plotted in Figure 9. The data, which extend the weld thickness to plate thickness ratio down to 0.09, deviate from theoretical curves passed through the points of largest weld width for both yield stress and ultimate tensile stress.

The hardness variations across a TIG and an EB weld of Figure 2 provide a clue toward an explanation of this deviation from theoretical behavior. The soft part of the heat-affected-zone of a weld does not shrink in proportion to the size of the fusion zone. Figure 10 shows how, with some scatter, the effective weld size parameter begins to deviate from the measured weld size parameter below weld width to plate thickness ratios around 0.5. The deviation takes the form of a leveling off of the effective weld parameter to a constant or slowly decreasing value as the fusion zone continues to decrease. It should be possible to compute the weld size parameter correction from combined heat transfer calculations and empirical hardness-temperature-time variation data.

The yield stress and ultimate tensile stress are plotted against an effective weld size parameter in Figure 11. The yield stress is brought into good agreement with theory by this correction but the ultimate tensile strength is not. To bring the ultimate tensile strength into good agreement would require:

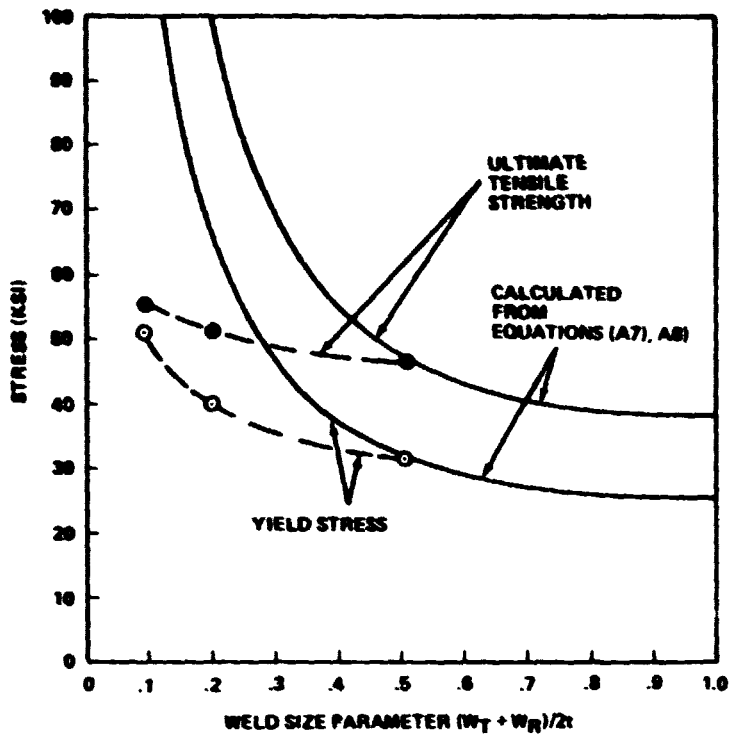


Figure 9. Comparison of data from Reference 14 with calculated dependence of yield stress and ultimate tensile strength on weld size parameter.

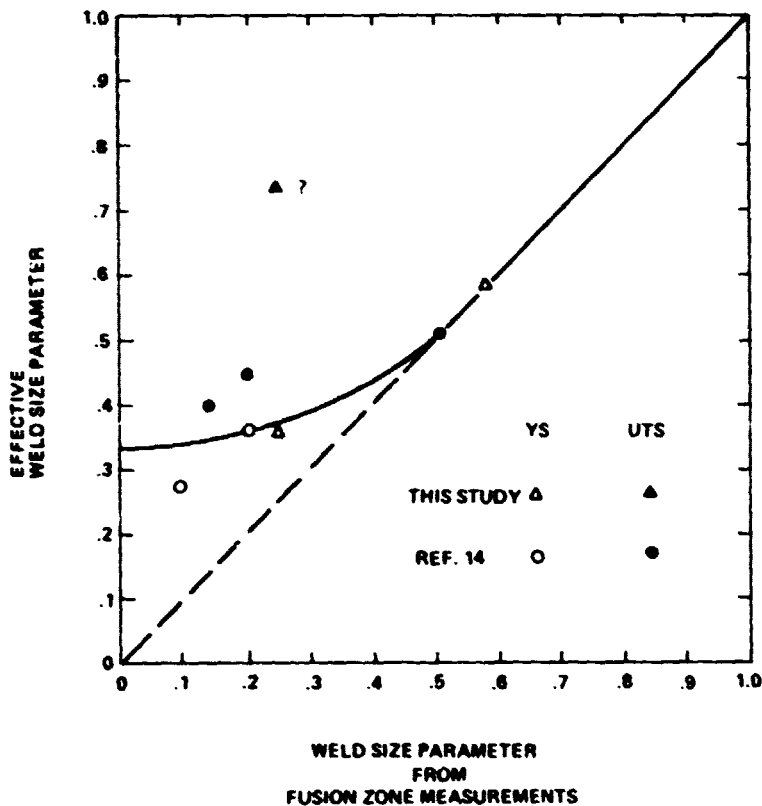


Figure 10. Effective versus measured weld size parameters.

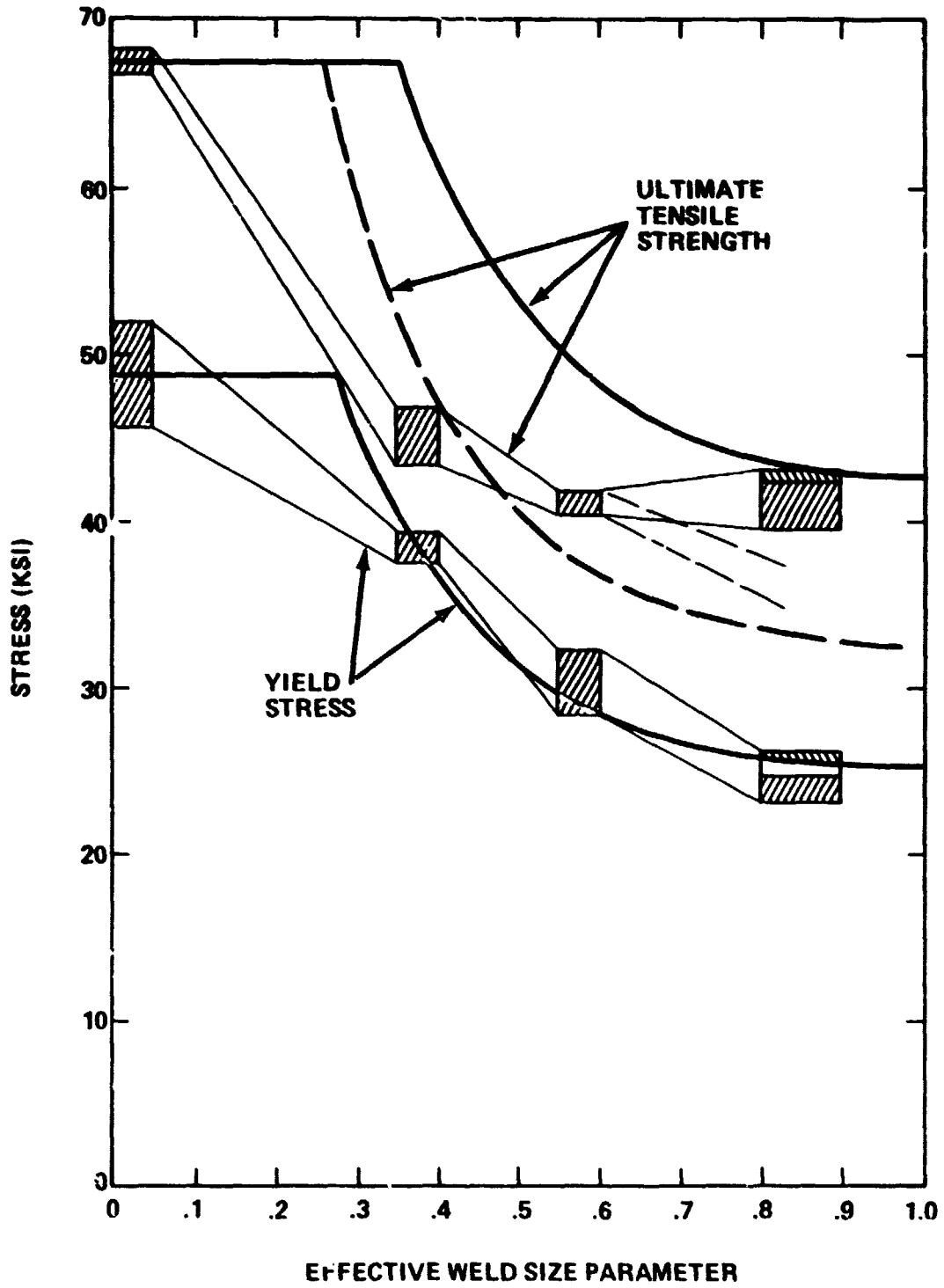


Figure 11. Yield stress and ultimate tensile strength data versus effective weld size parameter.

1) A larger correction of the measured weld size parameter for the ultimate tensile strength than for the yield stress when computing effective weld size parameters.

2) A smaller ultimate tensile strength for the EB weld metal than for the TIG weld metal, about 25 percent smaller by comparison of the broken versus the solid ultimate tensile strength line. This is why these points fall so far off the line in Figure 10.

It is possible to make arguments for both of the above assumptions:

1) Plastic flow in the soft weld zone between yielding and the attainment of the ultimate tensile strength would be expected to broaden the zone of plastic flow. Strain hardening of the softer inner layers of the weld zone would allow loading of initially harder outer layers to yielding.

2) A 25 percent reduction in tensile strength for the EB welds suggests 80 percent larger defects² (not affecting the yield stress) of the type initiating cracking leading to rupture. The rapid cooling of the EB welds combined with the possibility for contamination at interlayers between the stacked plates would seem to allow for more or larger defects. Reduction of work hardening rate would also reduce the ultimate tensile strength, but a rationale for such an effect is missing.

Thus, with empirical corrections, it is possible to explain the dependence of the weld joint strength in 1/4-in. 2219-T87 aluminum plate as a function of weld geometry (Figs. 12 and 13). This interpretation of the data must be regarded as tentative, however, pending a more detailed study.

The theory of the effect of weld geometry is able to explain the variation in weld strength on a purely geometrical basis without invoking metallurgical (microstructural) changes beyond widening or narrowing the weld width with two exceptions:

1) The EB welds (i.e., beads on plate) appear to differ from the TIG welds with respect to microstructure responsible for limiting the maximum load carrying capacity of the joint. This is considered a fault in experimental procedure rather than an effect that needs incorporation into the basic theory. The theory, of course, permits detection of such effects.

2) For very wide welds, i.e., welds wider than 1.7 times the plate thickness, softening of the heat-affected-zone in excess of that in the fusion zone is observed. This manifests itself in a reduced yield stress and a shift in location of fracture to the heat affected zone.

2. Assuming a fracture stress proportional to the inverse square root of the defect size.

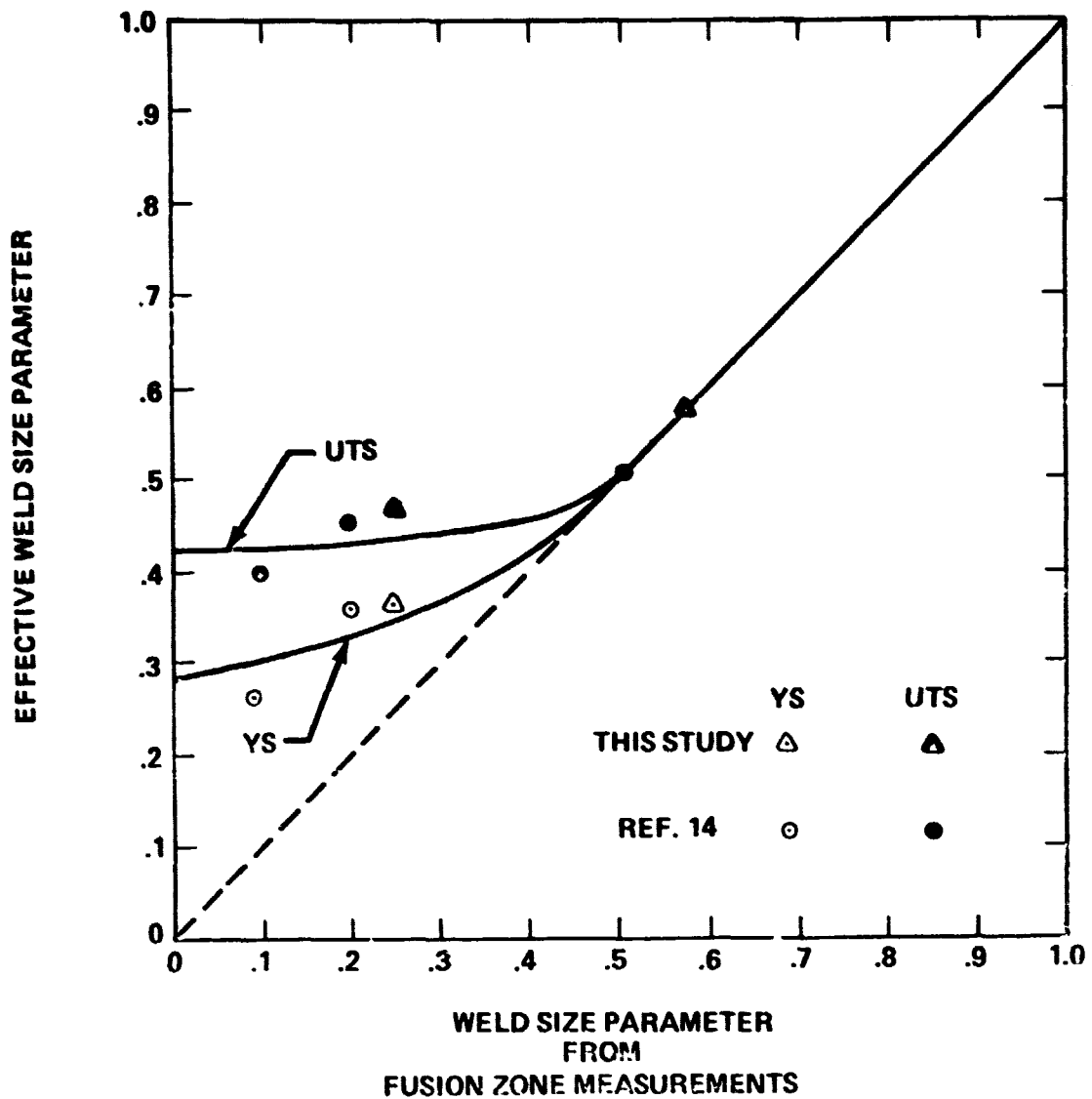


Figure 12. Weld size parameter corrections for yield stress and ultimate tensile strength.

The data showing the effect of heat sink or cooling rate capacity of the weld environment demonstrates that variations in cooling rate cannot be neglected as determinants of weld properties. The clear implication is that energy input alone is not determinative of weld properties. It is desirable, therefore, to use in preference to energy input a more determinative indicator of weld properties. Weld width, which is a function of both power input and cooling rate, suggests itself as a better indicator of weld quality than energy input. For a given weld speed, a weld width indicating adequate weld quality would, from this standpoint, be considered acceptable (pending other required tests) regardless of the weld power setting of the machine.

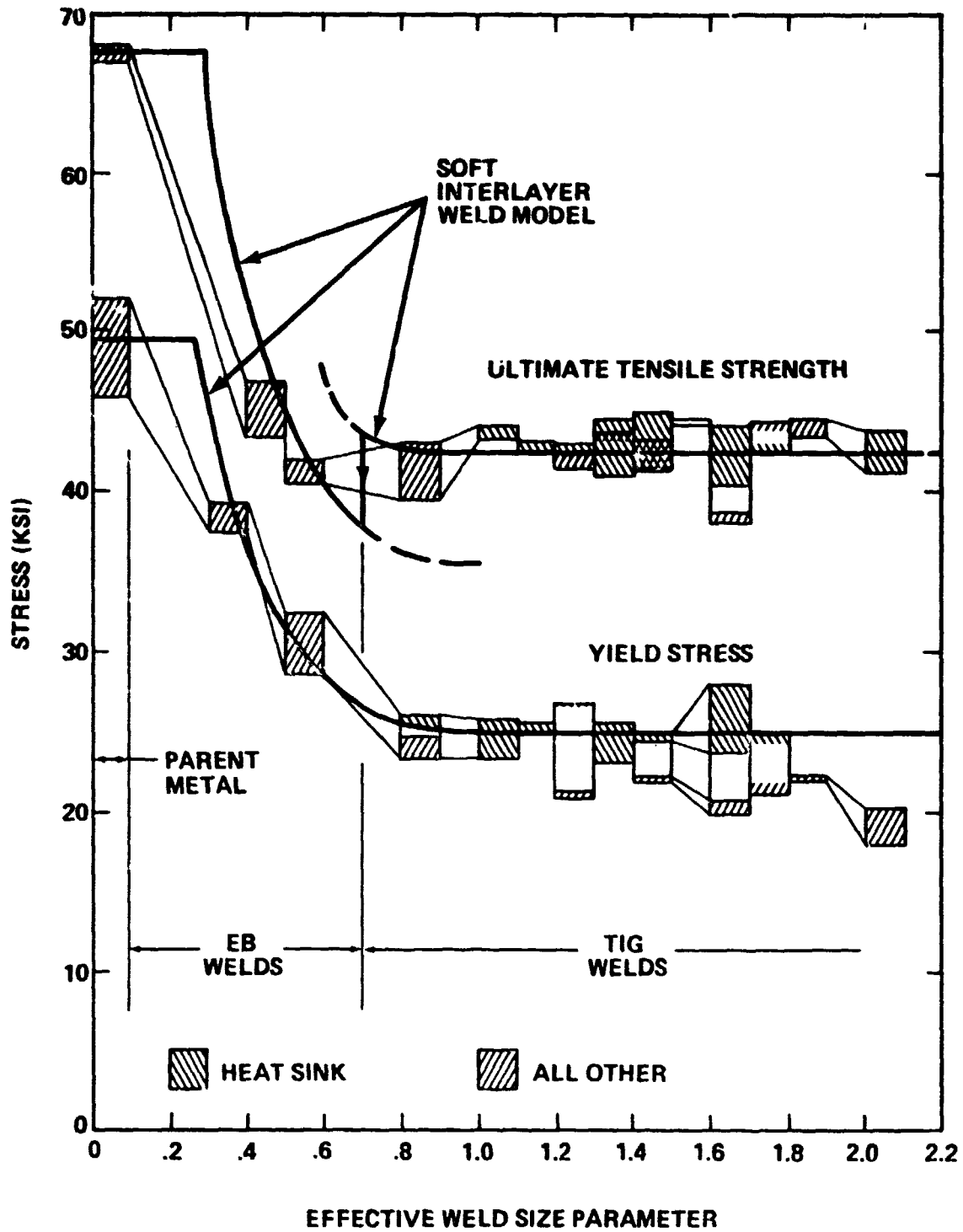


Figure 13. Interpretation of weld test data using soft interlayer weld model.

CONCLUSIONS

The soft interlayer theory of weld joint strength appears to explain the dependence of joint yield stress and ultimate tensile strength upon weld geometry for 1/4-in. butt welds in 2219-T87 aluminum.

If it is desired to determine metallurgical (microstructural) effects in welding processes, purely geometrical effects must be accounted for when weld geometry is allowed to change.

In 1/4-in. butt welds in 2219-T87 aluminum, the mechanical properties of the fusion zone appear to be constant and determinative of joint mechanical properties with two exceptions:

- 1) For very narrow welds (weld width less than half the plate thickness) the effective weld width is greater than the fusion zone for soft interlayer strength calculations, presumably because the soft regions of the heat-affected-zone do not reduce in proportion to the fusion zone.

- 2) For very wide welds (weld width greater than 1.7 times the plate thickness) softening of the heat-affected-zone in excess of that in the fusion zone lowers the yield stress of the joint and shifts the fracture to the heat-affected-zone.

Weld joint properties are functions of both the power input and cooling rate of the weld environment. Cooling rate is difficult to determine or even hold constant in many cases. Consequently, power input to a weld is only a rough determinant of mechanical properties at best.

The width of a weld, which can be observed as it is being made, appears to be a better indicator of weld joint mechanical properties than power input.

REFERENCES

1. Bakshi, O. A. and Shron, R. Z.: The Static Tensile Strength of Welded Joints with a Soft Interlayer. *Welding Production* vol. 9, No. 5, May 1962, pp. 9-15.
2. Bakshi, O. A., Monoshkov, A. N., and Anisimov, Yu. I: Efficiency of Welded Joints Containing a Soft Layer in Low Temperature Impact Tensile Tests. *Welding Production*, vol. 15, No. 5, November 1968, pp. 1-5.
3. Bakshi, O. A. and Bogomolova, A. S.: Strength of Mechanically Heterogeneous Welded Joints in Biaxial Tension. *Welding Production*, vol. 18, No. 5, May 1971, pp. 5-9.
4. Hill, R.: *The Mathematical Theory of Plasticity*. Oxford University Press, 1950 pp. 226-236. Note: The expressions developed for compression are reversible for the tensile case.
5. Bakshi, O. A.: Brittle Fracture on Welded Joints. *Automatic Welding*, vol. 19, No. 2, February 1966, pp. 20-25.
6. Cottrell, C. L. M.: Fracture Toughness Concepts Applied to the Zones of Welded Joints. *British Welding Journal*, vol. 15, No. 6, June 1968, pp. 262-267.
7. Kelly, A. and Nicholson, R. B.: Precipitation Hardening. *Progress in Materials Science*, vol. 10, 1963, pp. 149-391.
8. Broek, D.: The Role of Inclusions in Ductile Fracture and Fracture Toughness. *Engineering Fracture Mechanics*, vol. 5, No. 1, 1973, pp. 55-66.
9. Staley, J. T.: Microstructure and Toughness of High-Strength Aluminum Alloys. ASTM Special Technical Publication 605: Properties Related to Fracture Toughness, 1976, pp. 71-96.
10. Knott, J. F.: Micro-Mechanisms of Fracture and the Fracture Toughness of Engineering Alloys. *Advances in Research on the Strength and Fracture of Materials*, vol. 1, University of Waterloo Press, Waterloo, Canada, 1977, pp. 61-92.
11. Nunes, A. C., Jr.: Weld Puddle Physics. NASA/ASEE Summer Faculty Research Fellowship Program - Marshall Space Flight Center (University of Alabama - Auburn University) NASA Contract NGT-01-002-080 Report August 1975. Note: Undulations in the root of a partial penetration TIG weld in quarter inch 2219-T87 aluminum plate shown in Figure 6 reveal sites of roughly 20 percent less penetration correlating in spacing with the holddown finger spacing on top of the clamping plate.

REFERENCES (Continued)

12. Shultz, B. L. and Jackson C. E.: Influence of Weld Bead Area on Weld Metal Mechanical Properties. *Welding Journal*, vol. 52, No. 1, January 1973, pp. 26-s to 37-s.
13. Stüwe, H. P.: The Work Necessary to Form a Ductile Fracture Surface. *Engineering Fracture Mechanics*, vol. 13, No. 2, February 1978, pp. 231-236.
14. Brennecke, M. W.: Electron Beam Welded Heavy Gage Aluminum Alloy 2219. *Welding Journal*, vol. 44, No. 1, January 1965, pp. 27-s to 39-s.
15. Prandtl, L.: Anwendungsbeispiele zu einem Henckyschen Satz über das plastische Gleichgewicht. *Zeitschrift für Angewandte Mathematik und Mechanik*, vol. 3, No. 6, December 1923, pp. 401-406.
16. Kachanov, L. M.: *Foundations of the Theory of Plasticity*. American Elsevier Publishing Co., Inc. 1971, pp. 228-231.

APPENDIX A
SOFT INTERLAYER WELD MODEL

Weld joints in metals which soften when exposed to welding conditions may be treated as a soft interlayer inside relatively hard parent metal (Fig. A-1).

If the weld is wider than the thickness of the parent metal plate, the joint yields at the yield stress σ_{yw} of the relatively soft weld metal. The joint ultimate tensile strength is also the same as that of the weld metal, σ_{uw} . The harder material surrounding the weld metal functions as grips for a tensile specimen of the softer metal. In summary, if w and t are the weld width and plate thickness respectively, and if σ_y and σ_u are the yield and ultimate tensile strengths of the joint, for $w \geq t$:

$$\sigma_y = \sigma_{yw} \quad , \quad (A-1)$$

$$\sigma_u = \sigma_{uw} \quad . \quad (A-2)$$

If the weld width is less than the plate thickness, then the easiest (45 degree) slip planes are blocked by the harder parent metal outside the weld. The planes crossing the weld diagonally (corner to corner) become the easiest slip planes, assuming that the parent metal is substantially harder than the weld metal. If the mean tensile stress on the weld is σ , the shear force on a unit length of diagonal plane F_s is (Fig. A-2):

$$F_s = \sigma t \left(\frac{W}{\sqrt{W^2 + t^2}} \right) \quad . \quad (A-3)$$

The area of the diagonal plane A_d is:

$$A_d = \sqrt{w^2 + t^2} \quad . \quad (A-4)$$

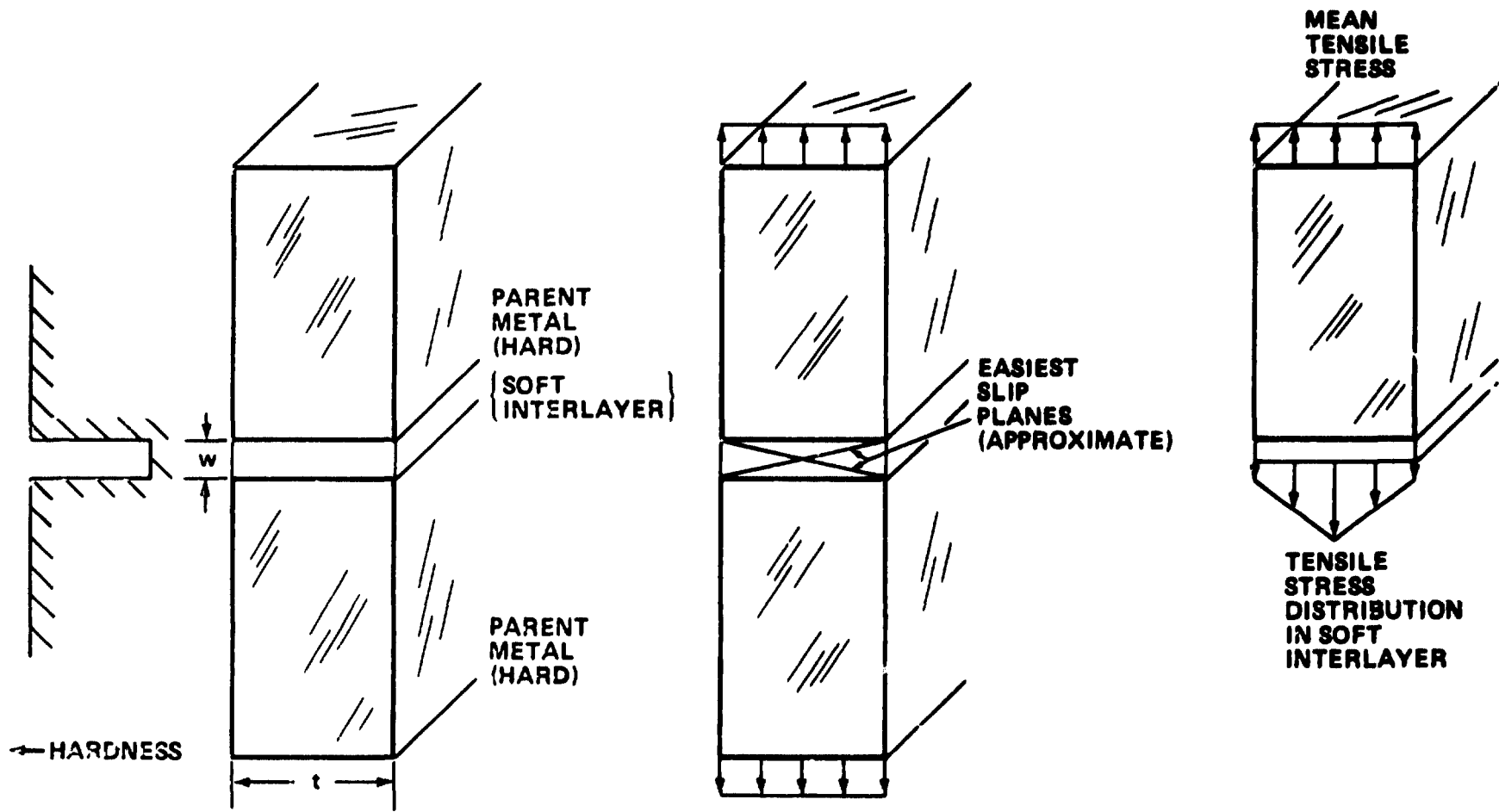


Figure A-1. Soft interlayer weld model.

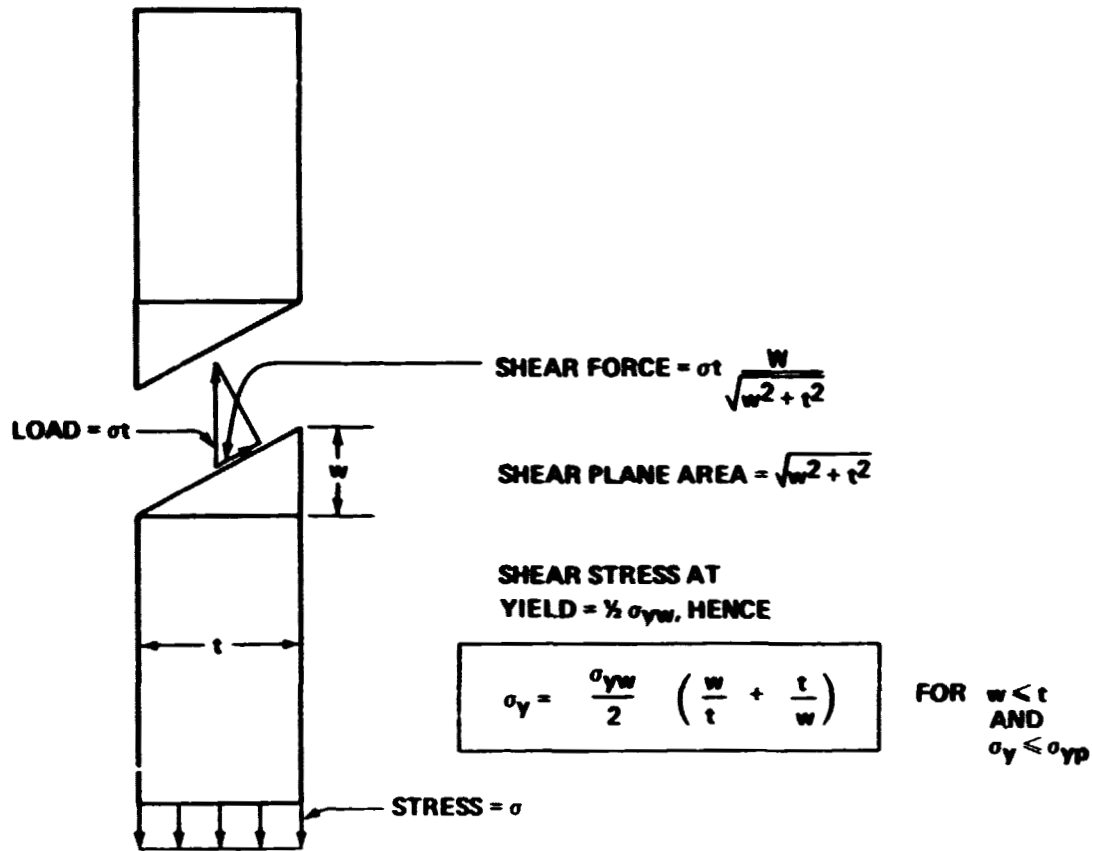


Figure A-2. Yield stress of soft interlayer joint.

The shear stress τ_d on the diagonal plane is:

$$\tau_d = \frac{F_s}{A_d} = \sigma t \left(\frac{W}{W^2 + t^2} \right) = \left(\frac{\sigma}{\frac{W}{t} + \frac{t}{W}} \right) \quad (A-5)$$

At yield (maximum shear criterion):

$$\tau_d = \frac{1}{2} \sigma_{yw} \quad (A-6)$$

Hence, for $w \leq t$,

$$\sigma_y = \frac{\sigma_{yw}}{2} \left(\frac{w}{t} + \frac{t}{w} \right) \quad (A-7)$$

Assuming that the processes leading to limiting of load bearing capacity and fracture take place on the more difficult diagonal slip plane just as they would have on the 45 degree slip planes under the action of the shear stress resolved on the slip plane, then the ultimate tensile stress should be proportional to the yield stress and for $w \leq t$,

$$\sigma_u = \frac{\sigma_{uw}}{2} \left(\frac{w}{t} + \frac{t}{w} \right) \quad (A-8)$$

If the width of the fusion zone of the weld is W_T at the top and W_R at the root (Fig. A-3), an equivalent interlayer thickness giving the correct slip plane angle for use in the above calculations is the simple average thickness:

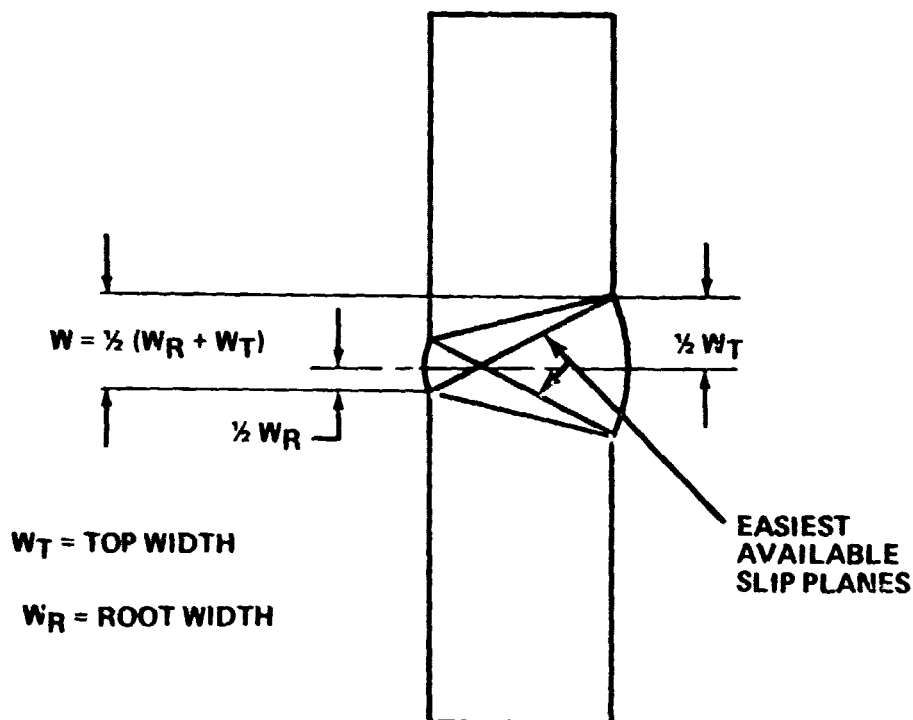


Figure A-3. Equivalent width of weld.

$$W = \frac{1}{2} (W_T + W_R) \quad . \quad (A-9)$$

To account for the softened heat-affected-zone regions, some broadening of the equivalent W beyond the fusion zone should improve results.

After yielding along the diagonal planes occurs the plastic flow field develops as shown in Figure A-4. The slip lines, for a fully developed plastic flow, spread to the boundary of the soft interlayer for a substantial length compared to the thickness of the plate. Under these conditions, Prandtl's [15] classic plastic flow model for the compression of a plastic slab can be applied with the loading reversed to tension. A mean tensile stress σ across the soft interlayer generates a maximum tensile stress σ_{max} within the soft layer. When σ_{max} reaches the fracture stress σ_{fw} of the weld metal the joint ruptures.

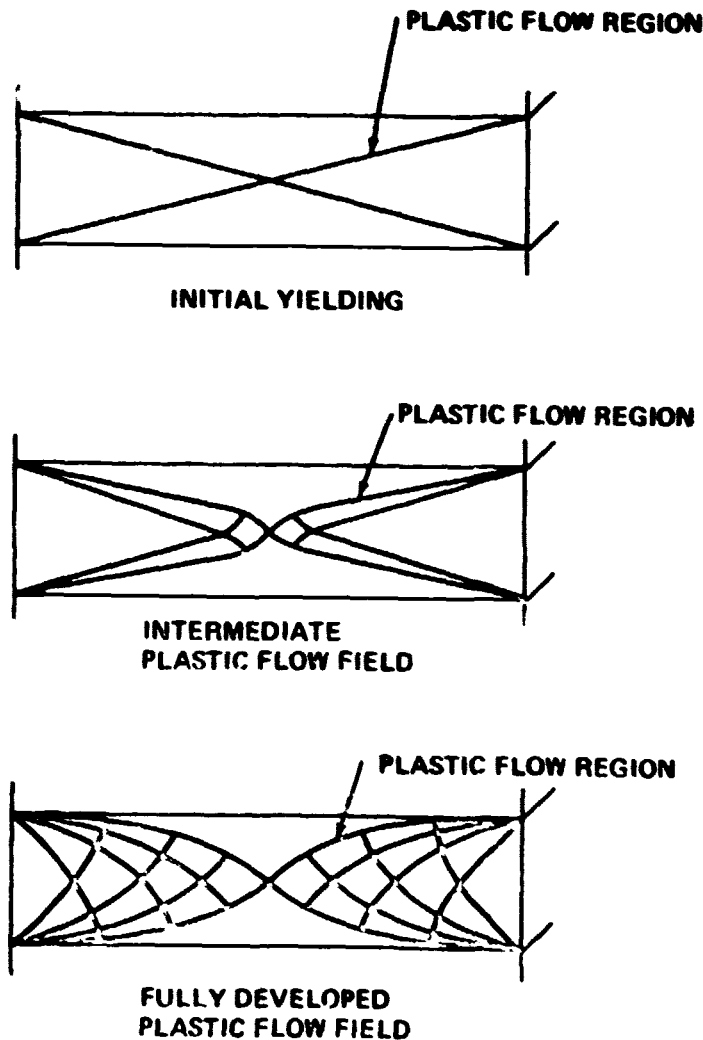


Figure A-4. Development of plastic flow field in soft interlayer under tension. Slip-lines, along which slip takes place, are shown.

Figure A-5 shows the geometry and boundary conditions to be used in the analysis.

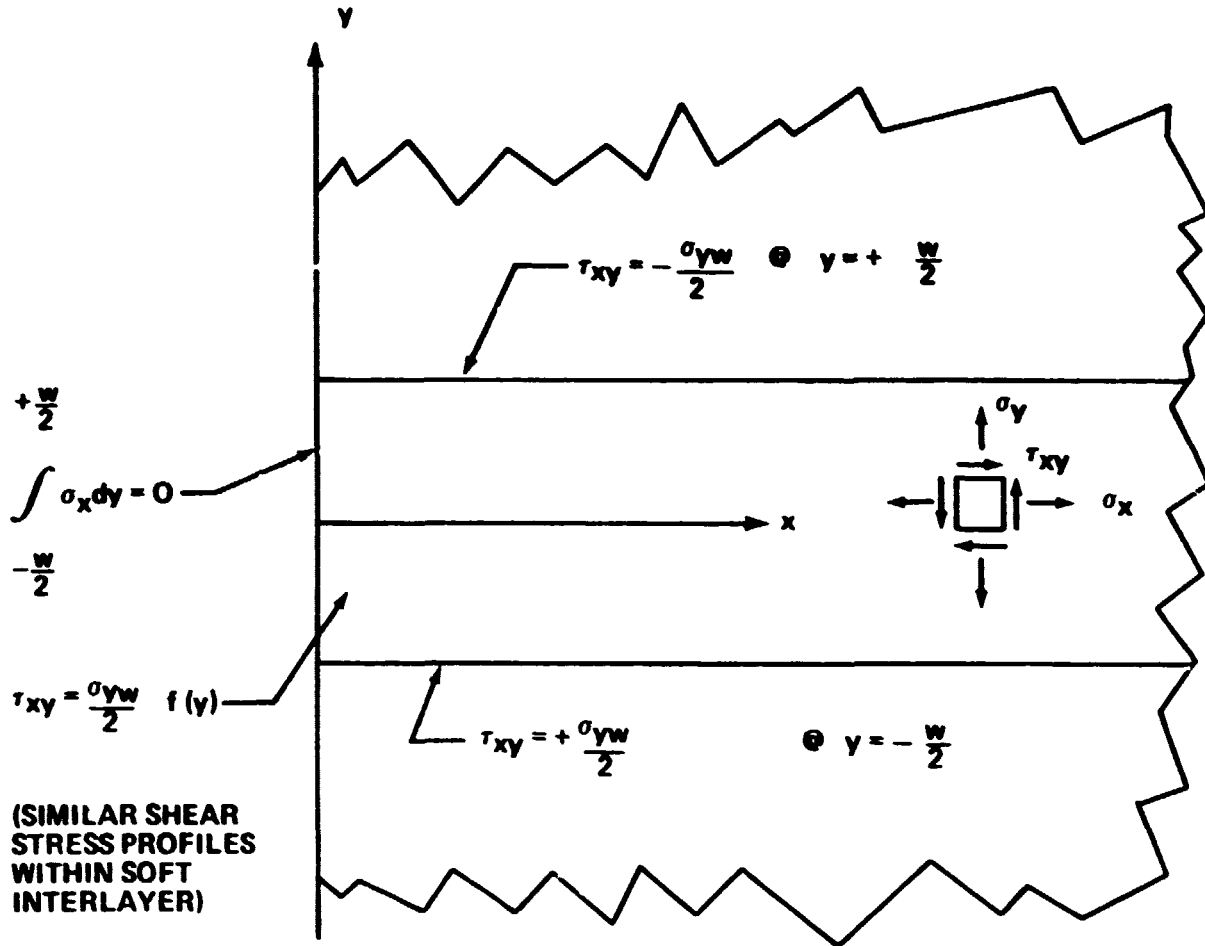


Figure A-5. Geometry and boundary conditions assumed for Prandtl analysis of fully developed plastic flow field.

X- and Y-direction equilibrium of a small element of the plastically deforming field requires that:

$$\frac{\partial \sigma_x}{\partial x} + \frac{\partial \tau_{xy}}{\partial y} = 0 \quad , \quad (A-10)$$

$$\frac{\partial \sigma_y}{\partial y} + \frac{\partial \tau_{xy}}{\partial x} = 0 \quad . \quad (A-11)$$

Each element of the plastic field is assumed to have a plane passing through it in some direction stressed to the yield stress in shear. The yield stress in shear of the weld metal is taken as half the tensile yield σ_{yw} in accordance with the maximum shear yield criterion. Mohr's circle for a yielding element has a radius equal to the yield stress so that the maximum shear will come out to be the yield stress as shown in Figure A-6. The stresses of the yielding element are related:

$$\left(\frac{\sigma_x - \sigma_y}{2}\right)^2 + (\tau_{xy})^2 = \left(\frac{\sigma_{yw}}{2}\right)^2 \quad (A-12)$$

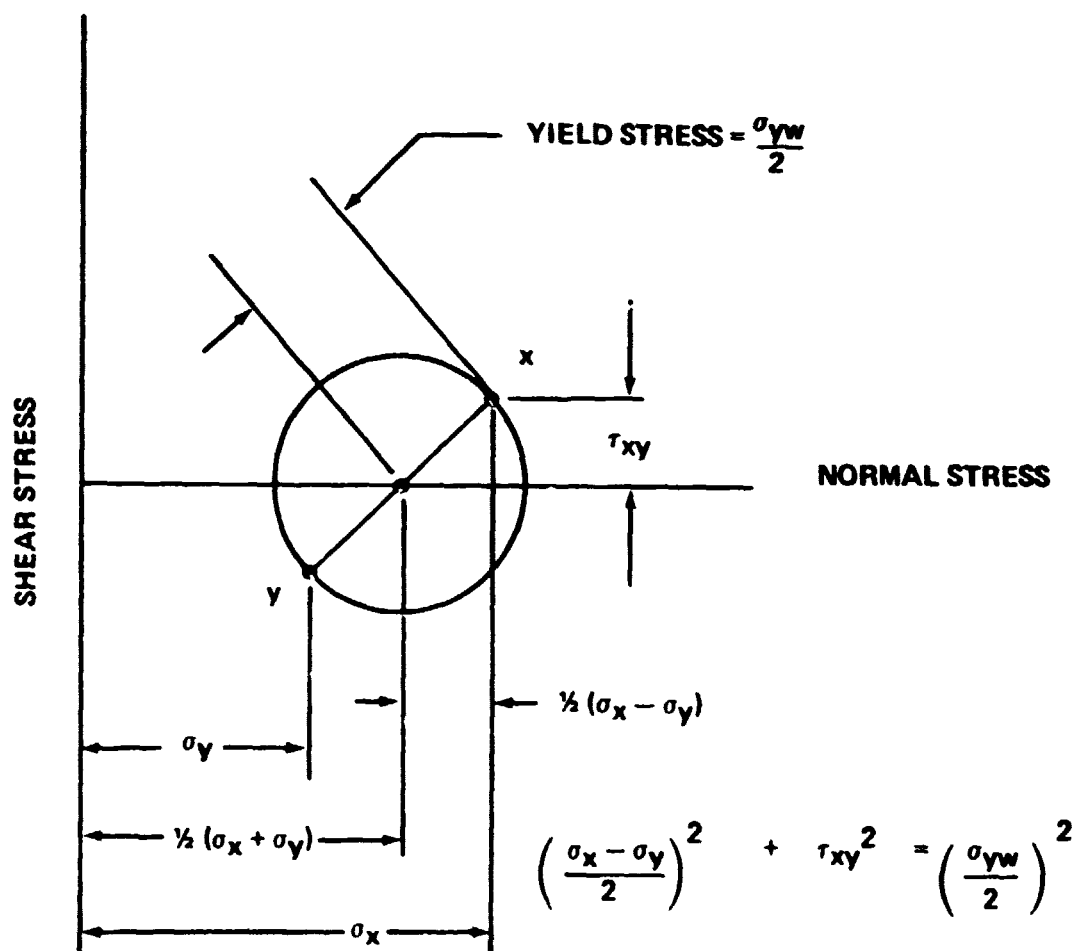


Figure A-6. Mohr's circle for stress transformation of yielding element.

at The boundary surfaces $y = \pm W/2$ are shearing surfaces, consequently

$$\text{at } y = \pm \frac{W}{2} \quad \tau_{xy} = \pm \frac{\sigma_{yw}}{2} \quad . \quad (\text{A-13})$$

The shear stress in between i.e., for $-W/2 < +W/2$, is assumed to vary with y in a shear stress profile independent of position x along the flow so that for

$$-\frac{W}{2} \leq y \leq +\frac{W}{2} \quad \tau_{xy} = -\frac{\sigma_{yw}}{2} \cdot f(y) \quad , \quad (\text{A-14})$$

where

$$f\left(+\frac{W}{2}\right) = 1 \quad , \quad (\text{A-15})$$

and

$$f\left(-\frac{W}{2}\right) = -1 \quad . \quad (\text{A-16})$$

Combining equations (A-10), and (A-14) yields:

$$\frac{\partial \sigma_x}{\partial x} - \frac{\sigma_{yw}}{2} \frac{\partial f}{\partial y} = 0 \quad , \quad (\text{A-17})$$

rewriting equation (A-12):

$$\sigma_x - \sigma_y = \pm \frac{\sigma_{yw}}{2} \sqrt{1 - f(y)^2} \quad , \quad (\text{A-18})$$

and differentiating both sides of equation (A-18) with respect to x yields the relation:

$$\frac{\partial \sigma_x}{\partial x} = \frac{\partial \sigma_y}{\partial x} \quad , \quad (\text{A-19})$$

which allows replacement of σ_x in equation (A-17) with σ_y :

$$\frac{\partial \sigma_y}{\partial x} - \frac{\sigma_{yw}}{2} \frac{df}{dy} = 0 \quad . \quad (\text{A-20})$$

Combining equations (A-14), and (A-11):

$$\frac{\partial \sigma_y}{\partial y} = 0 \quad . \quad (\text{A-21})$$

Since

$$\frac{\partial^2 \sigma_y}{\partial y \partial x} = \frac{\partial^2 \sigma_y}{\partial x \partial y} = 0 \quad , \quad (\text{A-22})$$

partial differentiation of equation (A-20) with respect to y requires:

$$\frac{d^2 f}{dy^2} = 0 \quad , \quad (\text{A-23})$$

or

$$f(y) = a y + b \quad , \quad (\text{A-24})$$

where a and b are constants. Inserting equation (A-21) into equations (A-15) and (A-16) requires:

$$f(y) = \frac{2y}{W} \quad . \quad (\text{A-25})$$

Combining equations (A-2.i) and (A-20):

$$\frac{d\sigma_y}{dx} = \frac{\sigma_{yw}}{W} \quad , \quad (\text{A-26})$$

and

$$\sigma_y = \sigma_{yw} \left(\frac{x}{W} + c \right) \quad , \quad (\text{A-27})$$

where c is a constant of integration. From equations (A-27), (A-25), (A-14), and (A-12):

$$\sigma_x = \sigma_{yw} \left(\frac{x}{W} + c - \sqrt{1 - \frac{4y^2}{W^2}} \right) \quad . \quad (\text{A-28})$$

At $x = 0$, the end force on the plastic layer vanishes in the x -direction or at $x = 0$:

$$\int_{y = -\frac{W}{2}}^{y = +\frac{W}{2}} \sigma_x dy = 0 \quad . \quad (\text{A-29})$$

Insertion of equation (A-28), into equation (A-29) allows evaluation of c :

$$c = \frac{1}{4} \quad . \quad (\text{A-30})$$

The stress field inside the plastically flowing soft interlayer is approximated:

$$\sigma_x = \sigma_{yw} \left(\frac{\pi}{4} + \frac{x}{W} - \sqrt{1 - \frac{4y^2}{W^2}} \right) , \quad (\text{A-31})$$

$$\sigma_y = \sigma_{yw} \left(\frac{\pi}{4} + \frac{x}{W} \right) , \quad (\text{A-32})$$

and

$$\tau_{xy} = \sigma_{yw} \left(-\frac{y}{W} \right) . \quad (\text{A-33})$$

The highest tensile stresses in the Prandtl analysis occur at the interface between the soft interlayer and the hard surrounding material at $x = t/2$ and $y = t/2$. These stresses are taken to be spurious because they are not found in the slip-line analysis of the problem. In the slip-line field analysis there is a non-deforming region adjacent to the boundary of the soft interlayer. The maximum tensile stresses occur on the centerline at $x = t/2$ and $y = 0$. The corresponding stresses obtained from the Prandtl analysis are:

$$\sigma_{\max} = \sigma_{yw} \left(\frac{\pi}{4} + \frac{t}{2W} \right) . \quad (\text{A-34})$$

The mean stress $\bar{\sigma}$ is obtained from the relation:

$$\bar{\sigma} = \frac{\int_{x=0}^{x=t/2} \sigma_y dx}{(t/2)} , \quad (\text{A-35})$$

which computation yields:

$$\bar{\sigma} = \sigma_{yw} \left(\frac{\pi}{4} + \frac{t}{4W} \right) . \quad (\text{A-36})$$

A tensile stress amplification factor σ_{\max}/σ can then be computed:

$$\frac{\sigma_{\max}}{\sigma} = \left(\frac{2 + \pi \frac{W}{t}}{1 + \pi \frac{W}{t}} \right) . \quad (\text{A-37})$$

This amplification factor obtained from the Prandtl analysis is compared with one obtained by use of a slip-line analysis [16] in Figure A-7. The discrete slip-line solutions oscillate about the Prandtl solution. The agreement is close enough so that the Prandtl solution is accepted for present purposes.

Given a weld metal fracture stress σ_{fw} for tensile loading, the weld joint may be expected to fracture at stress σ_f :

$$\sigma_f = \sigma_{fw} \left(\frac{1 + \pi \frac{W}{t}}{2 + \pi \frac{W}{t}} \right) , \quad (\text{A-38})$$

because of the stress amplification inside the soft interlayer.

Putting together these results yields the picture presented in Figure A-8 of the strength of a weld joint as a function of weld thickness to plate thickness ratio.

The ultimate tensile strength σ_u is reached when the ability of a tensile specimen to work harden is no longer sufficient to compensate for area reduction occurring during extension of the specimen. The force F supported by the soft interlayer is; from equation (A-33):

$$F = \sigma_{yw} t \left(\frac{\pi}{4} + \frac{t}{W} \right) . \quad (\text{A-39})$$

Assuming constant volume for the soft interlayer

$$d (Wt) = 0 , \quad (\text{A-40})$$

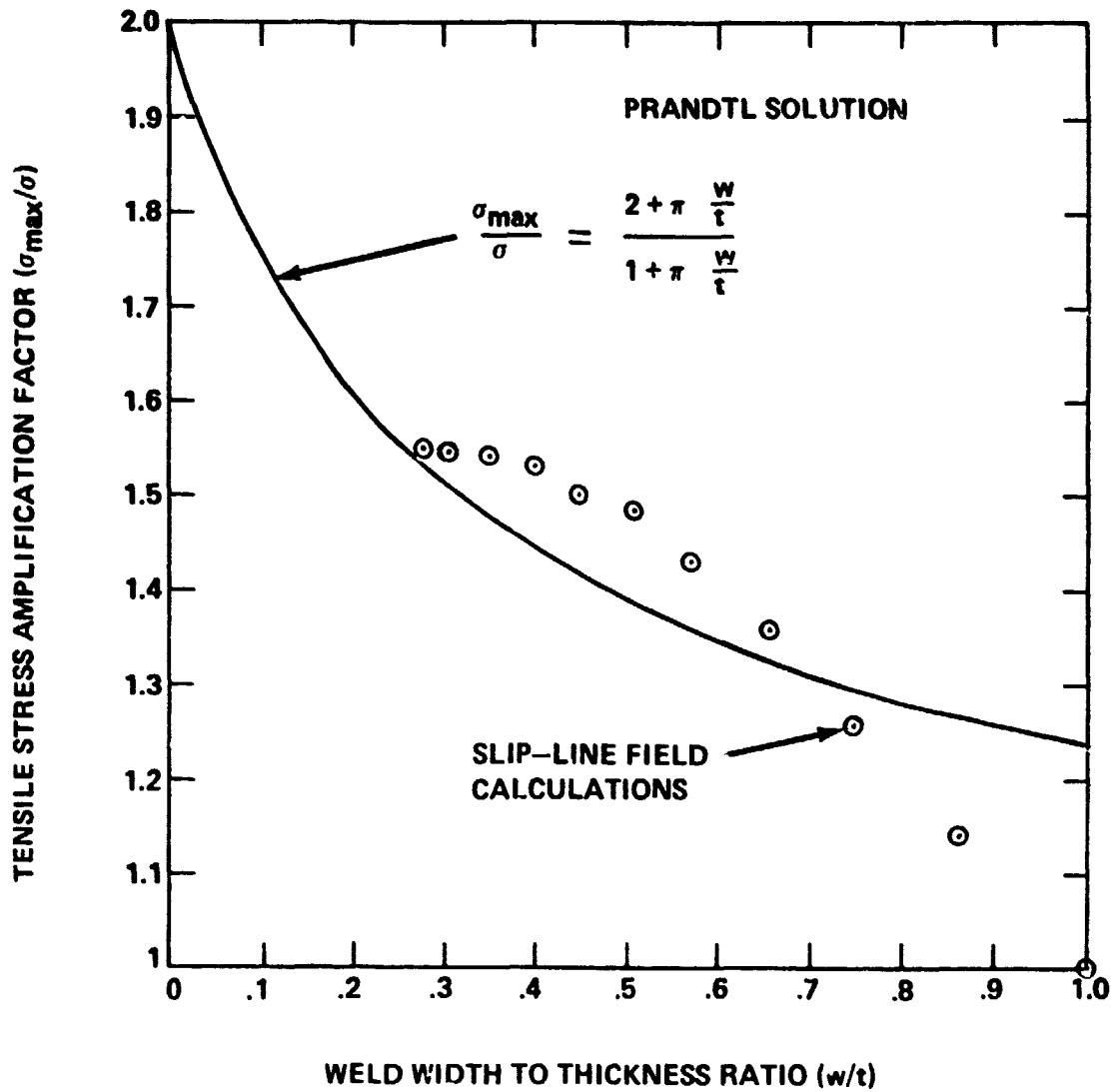


Figure A-7. Comparison of tensile stress amplification factor for soft interlayer as a function of weld width to plate thickness ratio calculated by Prandtl and slip-line field analyses.

at the ultimate tensile strength where

$$dF = 0 \quad , \quad (A-41)$$

then the work hardening condition at the ultimate tensile strength is:

$$\frac{d\sigma_{yw}}{dw} = \frac{\sigma_{yw}}{W} \quad . \quad (A-42)$$

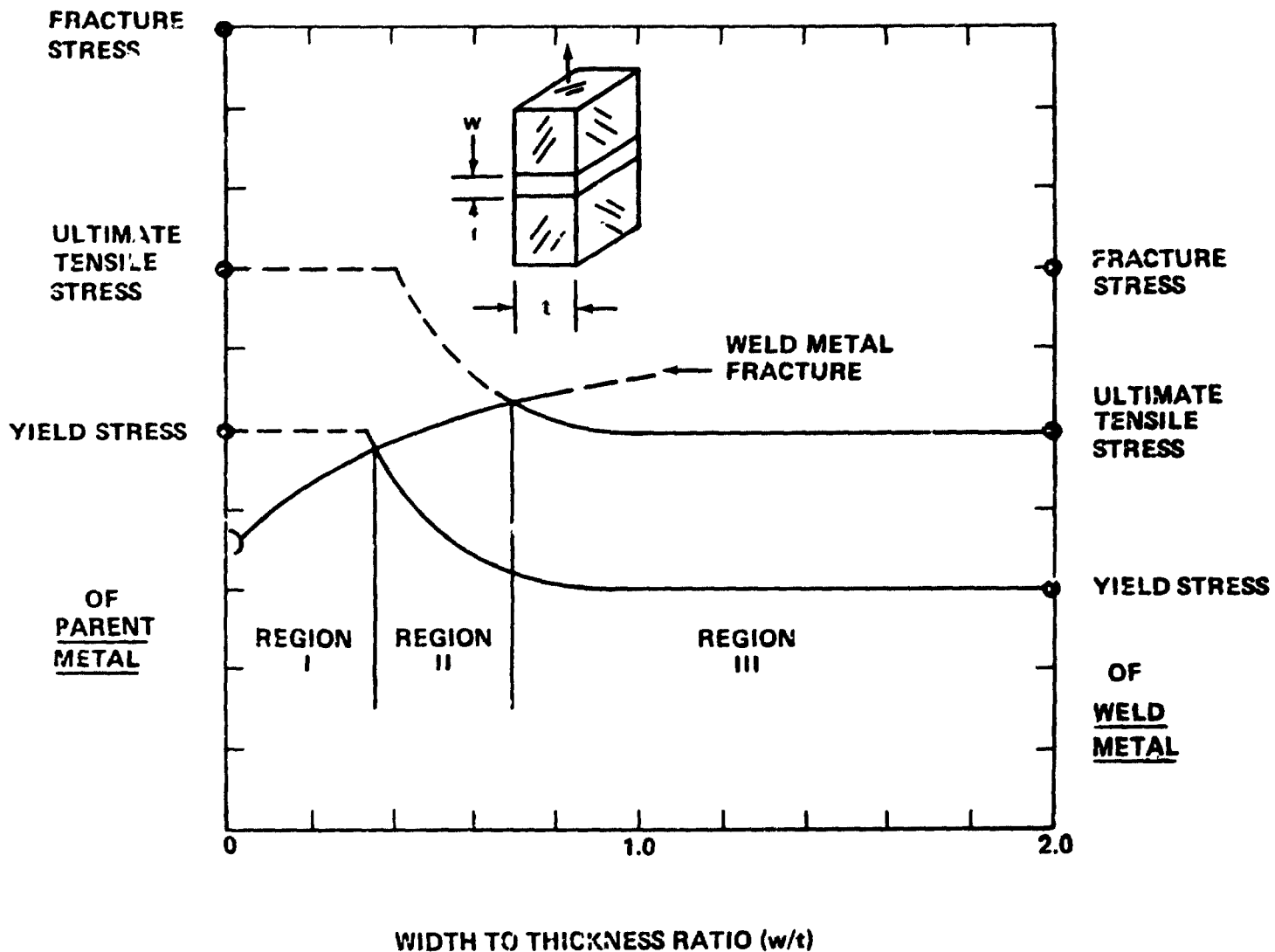



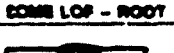


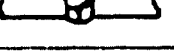










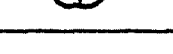










Figure A-8. Strength of weld joint obtained from strength of parent and weld metal using a simplified soft interlayer weld model.

Since the yield stress versus strain curve is what determines the ultimate tensile test for this geometry as for the typical tensile specimen the ultimate tensile strength should vary proportional to the yield stress as was assumed to derive the relation for the yield strength, equation (A-8).

APPENDIX B

DATA SHEETS

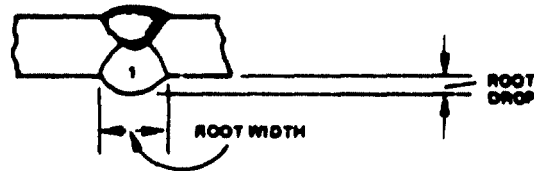
DATA SHEET TIG WELD 2219 - T07 AL. - WITH HEAT SINK

PANEL NO. (720)	TEST PACE (AMPS/VOLTS)	WELDER NO. - /AMP/V.	UTS (KSI)	Y.TS (KSI)	EL. % - 2"	ROOT WIDTH	ROOT DROP	LOCATION OF FRACTURE	COMMENTS: TYPICAL WELD SHAPES
P1-110-1	150/12.5	2 155/14	29.2	23.5	2.2	.038	.038	LOP Q BREAK TOE - TOE	 12.3K JOULE ROOT PASS
P1-110-2	150/12.5	2 155/14	43.1	23.3	3.5	.046	.038	LOP Q BREAK TOE - TOE	 12.3K JOULE ROOT PASS
P1-110-3	150/12.5	2 155/14	22.4	23.3	3.0	.106	.038	LOP Q BREAK TOE - TOE	 12.3K JOULE ROOT PASS
P1-110-4	150/12.5	2 155/14	42.4	23.4	2.8	.093	.038	LOP Q BREAK TOE - TOE	 12.3K JOULE ROOT PASS
P1-120-1	175/12.5	2 155/14	43.7	23.2	2.8	.122	.038	TOE - TOE	 14.6 K JOULE ROOT PASS
P1-120-2	175/12.5	2 155/14	43.4	23.9	4.0	.138	.038	TOP Q TO TOE	 14.6 K JOULE ROOT PASS
P1-120-3	175/12.5	2 155/14	43.3	28.1	3.5	.197	.031	TOP Q TO TOE	 14.6 K JOULE ROOT PASS
P1-120-4	175/12.5	2 155/14	43.7	-	4.5	.196	.047	TOP Q TO TOE	 14.6 K JOULE ROOT PASS
P1-130-1	150/12.5	2 155/14	42.4	28.5	4.0	.238	.058	TOP Q TO TOE	 15.8 K JOULE ROOT PASS
P1-130-2	150/12.5	2 155/14	43.1	25.8	4.0	.254	.088	TOP Q TO TOE	 15.8 K JOULE ROOT PASS
P1-130-3	150/12.5	2 155/14	42.9	28.5	4.5	.271	.094	TOP Q TO TOE	 15.8 K JOULE ROOT PASS
P1-130-4	150/12.5	2 155/14	42.9	28.5	4.0	.268	.060	TOP Q TO TOE	 15.8 K JOULE ROOT PASS
P3-145-1	215/12.5	2,3 148/14	42.5	23.8	2.8	.323	.088	TOP Q TO TOE	 18.2 K JOULE ROOT PASS
P3-145-2	215/12.5	2,3 148/14	41.0	23.3	3.5	.361	.071	TOP Q TO TOE	 18.2 K JOULE ROOT PASS
P3-145-3	215/12.5	2,3 148/14	41.4	24.2	2.5	.375	.073	TOP Q TO TOE	 18.2 K JOULE ROOT PASS
P3-145-4	215/12.5	2,3 148/14	41.1	22.7	4.0	.370	.070	TOP Q TO TOE	 18.2 K JOULE ROOT PASS
P3-150-1	225/12.5	2,3 148/14	45.0	24.3	4.5	.373	.075	TOP Q TO TOE INTERFACE	 21.2K JOULE ROOT PASS
P3-150-2	225/12.5	2,3 148/14	42.9	25.3	4.3	.373	.078	TOP Q TO TOE INTERFACE	 21.2K JOULE ROOT PASS
P3-150-3	225/12.5	2,3 148/14	44.4	25.5	4.5	.371	.075	TOP Q TO TOE INTERFACE	 21.2K JOULE ROOT PASS
P3-150-4	225/12.5	2,3 148/14	43.3	25.8	4.5	.375	.075	TOP Q TO TOE INTERFACE	 21.2K JOULE ROOT PASS
P3-175-1	275/12.5	2,3 148/14	43.3	25.2	2.5	.413	.075	INTERFACE	 23K JOULE ROOT PASS
P3-175-2	275/12.5	2,3 148/14	44.4	-	4.0	.415	.081	INTERFACE	 23K JOULE ROOT PASS
P3-175-3	275/12.5	2,3 148/14	44.2	-	4.0	.421	.038	COMB EDGES-INT-TOE	 23K JOULE ROOT PASS
P3-175-4	275/12.5	2,3 148/14	44.9	25.7	5.0	.420	.038	COMB EDGES-INT-TOE	 23K JOULE ROOT PASS
F5-120-1	225/12.5	2,3,4 120/14.5	42.7	25.9	3.0	.475	.088	INTERFACE	 24K JOULE ROOT PASS
F5-120-2	225/12.5	2,3,4 120/14.5	42.5	24.7	3.0	.498	.088	INTERFACE	 24K JOULE ROOT PASS
F5-120-3	225/12.5	2,3,4 120/14.5	40.8	25.3	2.5	.477	.088	INTERFACE	24K JOULE ROOT PASS
F5-120-4	225/12.5	2,3,4 120/14.5	43.0	25.2	2.5	.480	.088	INTERFACE	24K JOULE ROOT PASS
F8-120-1	220/12.5	2,3,4 120/14.5	43.4	23.9	3.5	.471	.030	INTERFACE	25K JOULE ROOT PASS
F8-120-2	220/12.5	2,3,4 120/14.5	43.4	27.0	3.0	.468	.088	INTERFACE	25K JOULE ROOT PASS
F8-120-3	220/12.5	2,3,4 120/14.5	42.0	-	3.0	.484	.020	INTERFACE	25K JOULE ROOT PASS
F8-120-4	220/12.5	2,3,4 120/14.5	45.0	25.5	3.0	.485	.037	INTERFACE	25K JOULE ROOT PASS
F8-220-1	315/12.5	2,3,4 120/14.5	44.1	25.0	3.0	.452	.098	INTERFACE	25.3K JOULE ROOT PASS
F8-220-2	315/12.5	2,3,4 120/14.5	43.9	23.8	3.5	.468	.104	INTERFACE	25.3K JOULE ROOT PASS
F8-220-3	315/12.5	2,3,4 120/14.5	43.8	25.0	3.0	.456	.102	INTERFACE	25.3K JOULE ROOT PASS
F8-220-4	315/12.5	2,3,4 120/14.5	45.0	25.1	3.5	.460	.103	INTERFACE	25.3K JOULE ROOT PASS







RANGE			
HIGH	45.0	25.5	5.0
LOW	29.2	22.7	2.5

NOTE TRAVEL SPEED FOR

ALL PASSES - 9 IN./MIN. WELDING PERFORMED DOWNHAND
TESTING PERFORMED ON TIMIUS OLSEN - C0,000 # MACHINE

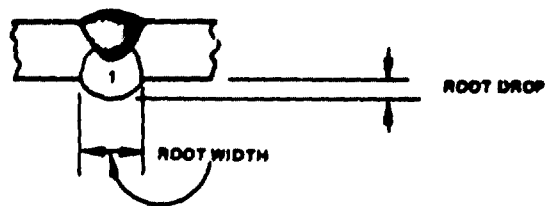


DATA SHEET TIG WELD 2219 - T87 AL. - NO HEAT SINK

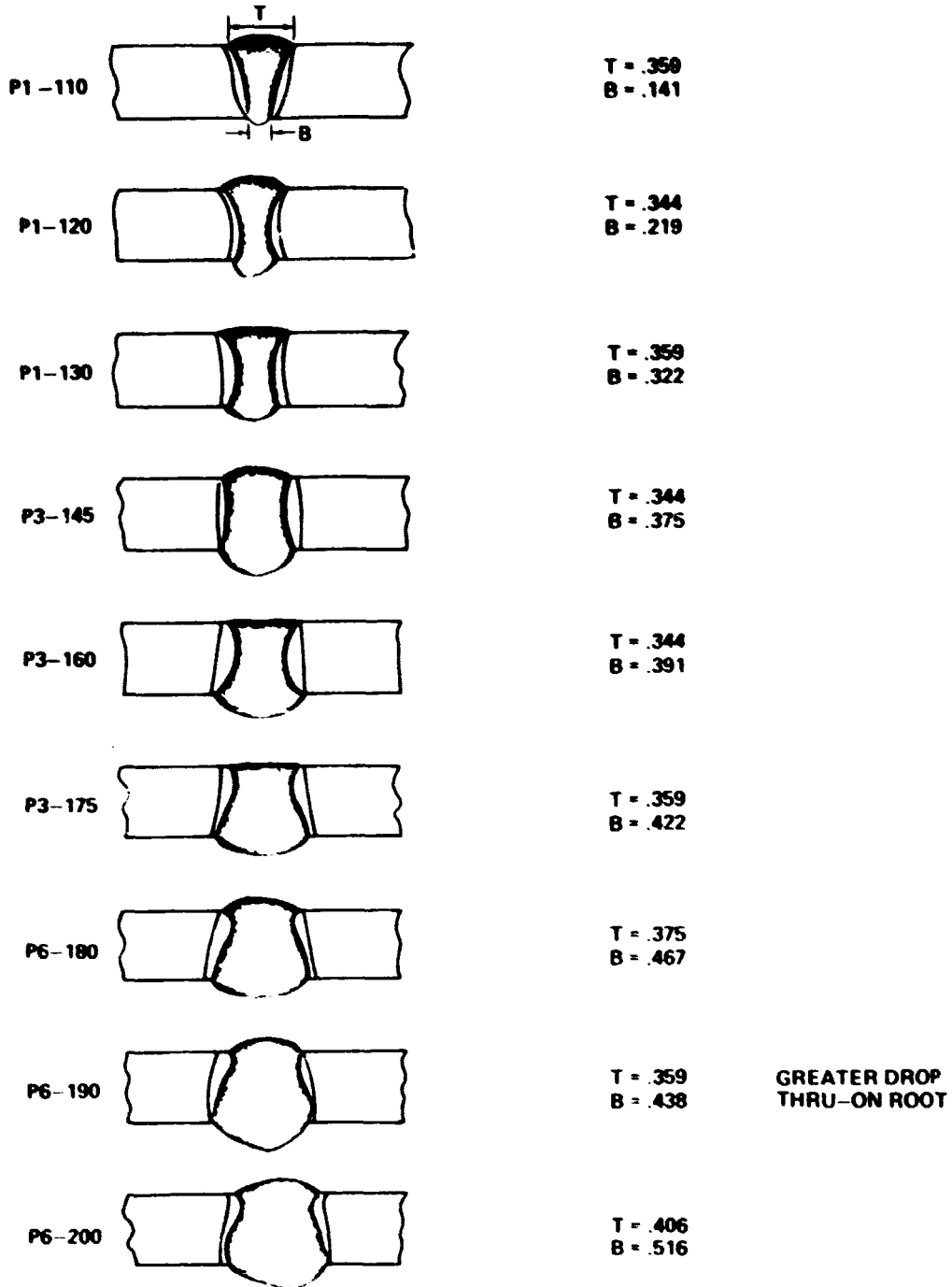
PANEL NO. (SPEC)	1ST PASS AMPS/VOLTS	(FILL) PASS NO - AMP/V.	UTS (KSI)	TYS (KSI)	EL. % - 2"	ROOT WIDTH"	ROOT DROP"	LOCATION OF FRACTURE	COMMENTS: TYPICAL WELD SHAPES
P480-1	120/12.5	2 120/14	43.0	24.9	4.5	.100	.034	INTERFACE -	 10K JOULE ROOT PASS SOME LOF. - ROOT
P480-2	120/12.5	2 120/14	42.8	23.2	4.0	.073	.021	TOE TO TOE	
P480-3	120/12.5	2 120/14	39.7	25.2	3.5	.106	.027	TOE TO TOE	
P480-4	120/12.5	2 120/14	35.2	25.2	2.5	.066	.020	LOF - Q BREAK	
P490-1	132/12.5	2 120/14	42.3	21.0	5.7	.239	.042	TOP Q - TOE	 11K JOULE ROOT PASS
P490-2	132/12.5	2 120/14	41.9	21.4	3.5	.251	.040	TOP Q - TOE	
P490-3	132/12.5	2 120/14	-	-	-	.268	.048	TOP Q - TOE	
P490-4	132/12.5	2 120/14	44.5	-	5.0	.265	.045	TOP Q - TOE	
P4100-1	148/12.5	2 120/14	43.3	21.9	4.8	.240	.080	INTERFACE	 12.5K JOULE ROOT PASS
P4100-2	148/12.5	2 120/14	43.4	-	5.6	.334	.049	INTERFACE	
P4100-3	148/12.5	2 120/14	41.7	21.8	5.0	.266	.080	INTERFACE	
P4100-4	148/12.5	2 120/14	42.3	20.8	5.8	.360	.061	INTERFACE	
P5110-1	160/12.5	2,3,4 120/14.5	38.0	19.8	3.5	.298	.078	INTERFACE	 13.5K JOULE ROOT PASS
P5110-2	160/12.5	2,3,4 120/14.5	38.3	20.4	3.5	.424	.090	INTERFACE	
P5110-3	160/12.5	2,3,4 120/14.5	38.8	20.9	3.0	.410	.093	INTERFACE	
P5110-4	160/12.5	2,3,4 120/14.5	40.0	23.1	4.8	.420	.093	INTERFACE	
P5120-1	175/12.5	2,3,4 120/14.5	44.4	21.4	5.5	.472	.090	OUTSIDE OF WELD	 14.5K JOULE ROOT PASS
P5120-2	175/12.5	2,3,4 120/14.5	44.6	22.0	5.0	.477	.098	ON TOP SIDE	
P5120-3	175/12.5	2,3,4 120/14.5	43.6	22.3	5.0	.485	.106	TOE TO TOE OF WELD	
P5120-4	175/12.5	2,3,4 120/14.5	42.3	20.9	4.5	.483	.103	SAME SIDE	
P5130-1	190/12.5	2,3,4 120/14.5	41.3	17.9	5.5	.537	.105	OUTSIDE OF WELD TO	 15.5K JOULE ROOT PASS
P5130-2	190/12.5	2,3,4 120/14.5	41.7	20.2	5.5	.538	.112	TOE - SAME SIDE	
P5130-3	190/12.5	2,3,4 120/14.5	43.7	20.2	7.5	.554	.112	INTERFACE	
P5130-4	190/12.5	2,3,4 120/14.5	43.2	20.3	5.5	.567	.114	OUTSIDE OF WELD TO	

RANGE			
HIGH	44.5	26.2	7.5
LOW	35.2	17.9	3.5

NOTE TRAVEL SPEED FOR ALL PASSES = 9 IN./MIN.
 WELDING PERFORMED DOWNHAND
 TESTING PERFORMED ON TINIUS OLSEN -
 60,000 # MACHINE
 PLATE WELDED WITH GRAIN & TESTED X GRAIN



RESULTS OF MACRO-ETCHING - WITH HEAT SINK (TOOLING)

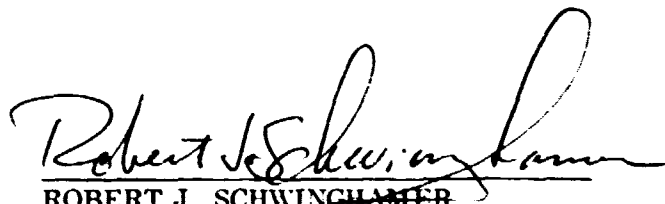


APPROVAL

**WELD GEOMETRY STRENGTH EFFECT IN
2219-T87 ALUMINUM**

**By A. C. Nunes, Jr., H. L. Novak, and
M. C. McIlwain**

The information in this report has been reviewed for technical content. Review of any information concerning Department of Defense or nuclear energy activities or programs has been made by the MSFC Security Classification Officer. This report, in its entirety, has been determined to be unclassified.



ROBERT J. SCHWINGLAMER

Director, Materials and Processes Laboratory